Intravascular optical coherence tomography [Invited]

BRETT E. BOUMA,[1,2,*] MARTIN VILLIGER,[1] KENICHIRO OTSUKA,[1] AND WANG-YUHL OH[3,4]

[1]*Harvard Medical School and Massachusetts General Hospital, Boston, MA 02171, USA*
[2]*Institute for Medical Engineering and Science, Cambridge, MA, 02139, USA*
[3]*Department of Mechanical Engineering, KAIST, 291 Daehak-ro, Yuseong-gu, Daejeon, South Korea*
[4]*KI for Health Science and Technology, KAIST, 291 Daehak-ro, Yuseong-gu, Daejeon, South Korea*
Bouma@mgh.harvard.edu

Abstract: Shortly after the first demonstration of optical coherence tomography for imaging the microstructure of the human eye, work began on developing systems and catheters suitable for intravascular imaging in order to diagnose and investigate atherosclerosis and potentially to monitor therapy. This review covers the driving considerations of the clinical application and its constraints, the major engineering milestones that enabled the current, high-performance commercial imaging systems, the key studies that laid the groundwork for image interpretation, and the clinical research that traces intravascular optical coherence tomography (OCT) from early human pilot studies to current clinical trials.

References

1. E. A. Swanson, J. A. Izatt, M. R. Hee, D. Huang, C. P. Lin, J. S. Schuman, C. A. Puliafito, and J. G. Fujimoto, "In vivo retinal imaging by optical coherence tomography," Opt. Lett. **18**(21), 1864–1866 (1993).
2. D. Huang, E. A. Swanson, C. P. Lin, J. S. Schuman, W. G. Stinson, W. Chang, M. R. Hee, T. Flotte, K. Gregory, C. A. Puliafito, and J. G. Fujimoto, "Optical coherence tomography," Science **254**(5035), 1178–1181 (1991).
3. M. E. Brezinski, G. J. Tearney, B. E. Bouma, J. A. Izatt, M. R. Hee, E. A. Swanson, J. F. Southern, and J. G. Fujimoto, "Optical coherence tomography for optical biopsy. Properties and demonstration of vascular pathology," Circulation **93**(6), 1206–1213 (1996).
4. D. Mozaffarian, E. Benjamin, A. Go, D. K. Arnett, M. J. Blaha, M. Cushman, S. R. Das, M. Sarah de Ferranti, J.-P. Després, and H. J. Fullerton, *AHA Statistical Update: Heart Disease and Stroke Statistics* (AHA, 2015).
5. E. Falk, P. K. Shah, and V. Fuster, "Coronary plaque disruption," Circulation **92**(3), 657–671 (1995).
6. R. T. Lee and P. Libby, "The unstable atheroma," Arterioscler. Thromb. Vasc. Biol. **17**(10), 1859–1867 (1997).
7. G. K. Sukhova, U. Schönbeck, E. Rabkin, F. J. Schoen, A. R. Poole, R. C. Billinghurst, and P. Libby, "Evidence for increased collagenolysis by interstitial collagenases-1 and -3 in vulnerable human atheromatous plaques," Circulation **99**(19), 2503–2509 (1999).
8. R. Virmani, F. D. Kolodgie, A. P. Burke, A. Farb, and S. M. Schwartz, "Lessons from sudden coronary death: a comprehensive morphological classification scheme for atherosclerotic lesions," Arterioscler. Thromb. Vasc. Biol. **20**(5), 1262–1275 (2000).
9. J. A. Condado, R. Waksman, O. Gurdiel, R. Espinosa, J. Gonzalez, B. Burger, G. Villoria, H. Acquatella, I. R. Crocker, K. B. Seung, and S. F. Liprie, "Long-term angiographic and clinical outcome after percutaneous trans-luminal coronary angioplasty and intracoronary radiation therapy in humans," Circulation **96**(3), 727–732 (1997).
10. P. S. Teirstein, V. Massullo, S. Jani, J. J. Popma, G. S. Mintz, R. J. Russo, R. A. Schatz, E. M. Guarneri, S. Steuterman, N. B. Morris, M. B. Leon, and P. Tripuraneni, "Catheter-based radiotherapy to inhibit restenosis after coronary stenting," N. Engl. J. Med. **336**(24), 1697–1703 (1997).
11. P. G. Yock and P. J. Fitzgerald, "Intravascular ultrasound: state of the art and future directions," Am. J. Cardiol. **81**(7 7A), 27E–32E (1998).
12. P. G. Yock, P. J. Fitzgerald, D. T. Linker, and B. A. Angelsen, "Intravascular ultrasound guidance for catheter-based coronary interventions," J. Am. Coll. Cardiol. **17**(6), 39–45 (1991).
13. F. M. Baer, P. Theissen, J. Crnac, M. Schmidt, M. Jochims, and H. Schicha, "MRI assessment of coronary artery disease," Rays **24**(1), 46–59 (1999).
14. G. G. Zimmermann-Paul, H. H. Quick, P. Vogt, G. K. von Schulthess, D. Kling, and J. F. Debatin, "High-resolution intravascular magnetic resonance imaging: monitoring of plaque formation in heritable hyperlipidemic rabbits," Circulation **99**(8), 1054–1061 (1999).

15. J. A. Rumberger, T. Behrenbeck, J. F. Breen, and P. F. Sheedy 2nd, "Coronary calcification by electron beam computed tomography and obstructive coronary artery disease: a model for costs and effectiveness of diagnosis as compared with conventional cardiac testing methods," J. Am. Coll. Cardiol. **33**(2), 453–462 (1999).

16. S. Motoyama, M. Sarai, H. Harigaya, H. Anno, K. Inoue, T. Hara, H. Naruse, J. Ishii, H. Hishida, N. D. Wong, R. Virmani, T. Kondo, Y. Ozaki, and J. Narula, "Computed tomographic angiography characteristics of atherosclerotic plaques subsequently resulting in acute coronary syndrome," J. Am. Coll. Cardiol. **54**(1), 49–57 (2009).

17. S. B. Puchner, T. Liu, T. Mayrhofer, Q. A. Truong, H. Lee, J. L. Fleg, J. T. Nagurney, J. E. Udelson, U. Hoffmann, and M. Ferencik, "High-risk plaque detected on coronary CT angiography predicts acute coronary syndromes independent of significant stenosis in acute chest pain: results from the ROMICAT-II trial," J. Am. Coll. Cardiol. **64**(7), 684–692 (2014).

18. Y. Uchida, F. Nakamura, T. Tomaru, T. Morita, T. Oshima, T. Sasaki, S. Morizuki, and J. Hirose, "Prediction of acute coronary syndromes by percutaneous coronary angioscopy in patients with stable angina," Am. Heart J. **130**(2), 195–203 (1995).

19. G. J. Tearney, S. A. Boppart, B. E. Bouma, M. E. Brezinski, N. J. Weissman, J. F. Southern, and J. G. Fujimoto, "Scanning single-mode fiber optic catheter-endoscope for optical coherence tomography," Opt. Lett. **21**(7), 543–545 (1996).

20. G. J. Tearney, M. E. Brezinski, S. A. Boppart, B. E. Bouma, N. Weissman, J. F. Southern, E. A. Swanson, and J. G. Fujimoto, "Images in cardiovascular medicine. Catheter-based optical imaging of a human coronary artery," Circulation **94**(11), 3013 (1996).

21. X. Li, T. H. Ko, and J. G. Fujimoto, "Intraluminal fiber-optic Doppler imaging catheter for structural and functional optical coherence tomography," Opt. Lett. **26**(23), 1906–1908 (2001).

22. B. Bouma, G. J. Tearney, S. A. Boppart, M. R. Hee, M. E. Brezinski, and J. G. Fujimoto, "High-resolution optical coherence tomographic imaging using a mode-locked Ti:Al$_2$O$_3$ laser source," Opt. Lett. **20**(13), 1486–1488 (1995).

23. B. E. Bouma, L. E. Nelson, G. J. Tearney, D. J. Jones, M. E. Brezinski, and J. G. Fujimoto, "Optical coherence tomographic imaging of human tissue at 1.55 μm and 1.81 μm using Er and Tm-doped fiber sources," J. Biomed. Opt. **3**(1), 76–79 (1998).

24. B. E. Bouma, G. J. Tearney, I. P. Bilinsky, B. Golubovic, and J. G. Fujimoto, "Self-phase-modulated Kerr-lens mode-locked Cr:forsterite laser source for optical coherence tomography," Opt. Lett. **21**(22), 1839–1841 (1996).

25. V. P. Yanovsky and F. W. Wise, "Frequency doubling of 100-fs pulses with 50% efficiency by use of a resonant enhancement cavity," Opt. Lett. **19**(23), 1952–1954 (1994).

26. K. F. Kwong, D. Yankelevich, K. C. Chu, J. P. Heritage, and A. Dienes, "400-Hz mechanical scanning optical delay line," Opt. Lett. **18**(7), 558–560 (1993).

27. G. J. Tearney, B. E. Bouma, and J. G. Fujimoto, "High-speed phase- and group-delay scanning with a grating-based phase control delay line," Opt. Lett. **22**(23), 1811–1813 (1997).

28. A. Rollins, S. Yazdanfar, M. Kulkarni, R. Ung-Arunyawee, and J. Izatt, "In vivo video rate optical coherence tomography," Opt. Express **3**(6), 219–229 (1998).

29. G. J. Tearney, M. E. Brezinski, B. E. Bouma, S. A. Boppart, C. Pitris, J. F. Southern, and J. G. Fujimoto, "In vivo endoscopic optical biopsy with optical coherence tomography," Science **276**(5321), 2037–2039 (1997).

30. J. G. Fujimoto, S. A. Boppart, G. J. Tearney, B. E. Bouma, C. Pitris, and M. E. Brezinski, "High resolution in vivo intra-arterial imaging with optical coherence tomography," Heart **82**(2), 128–133 (1999).

31. H. Yabushita, B. E. Bouma, S. L. Houser, H. T. Aretz, I.-K. Jang, K. H. Schlendorf, C. R. Kauffman, M. Shishkov, D.-H. Kang, E. F. Halpern, and G. J. Tearney, "Characterization of human atherosclerosis by optical coherence tomography," Circulation **106**, 1640–1645 (2002).

32. L. Di Vito, M. Agozzino, V. Marco, A. Ricciardi, M. Concardi, E. Romagnoli, L. Gatto, G. Calogero, L. Tavazzi, E. Arbustini, and F. Prati, "Identification and quantification of macrophage presence in coronary atherosclerotic plaques by optical coherence tomography," Eur. Heart J. Cardiovasc. Imaging **16**(7), 807–813 (2015).

33. G. J. Tearney, H. Yabushita, S. L. Houser, H. T. Aretz, I. K. Jang, K. H. Schlendorf, C. R. Kauffman, M. Shishkov, E. F. Halpern, and B. E. Bouma, "Quantification of macrophage content in atherosclerotic plaques by optical coherence tomography," Circulation **107**(1), 113–119 (2003).

34. G. J. Tearney, I. K. Jang, and B. E. Bouma, "Evidence of cholesterol crystals in atherosclerotic plaques by optical coherence tomography," Eur. Heart J. **24**, 1462 (2003).

35. G. J. Tearney, I. K. Jang, and B. E. Bouma, "Optical coherence tomography for imaging the vulnerable plaque," J. Biomed. Opt. **11**(2), 021002 (2006).

36. S. K. Nadkarni, M. C. Pierce, B. H. Park, J. F. de Boer, P. Whittaker, B. E. Bouma, J. E. Bressner, E. Halpern, S. L. Houser, and G. J. Tearney, "Measurement of collagen and smooth muscle cell content in atherosclerotic plaques using polarization-sensitive optical coherence tomography," J. Am. Coll. Cardiol. **49**(13), 1474–1481 (2007).

37. J. N. van der Sijde, A. Karanasos, M. Villiger, B. E. Bouma, and E. Regar, "First-in-man assessment of plaque rupture by polarization-sensitive optical frequency domain imaging in vivo," Eur. Heart J. **37**(24), 1932 (2016).

38. M. Villiger, A. Karanasos, J. Ren, N. Lippok, M. Shishkov, G. van Soest, S. Nadkarni, E. Regar, and B. Bouma, "Intravascular polarization sensitive optical coherence tomography in human patients," in *CLEO: Applications and Technology* (Optical Society of America, 2016), AW1O. 2.

39. G. S. Abela and K. Aziz, "Cholesterol crystals cause mechanical damage to biological membranes: a proposed mechanism of plaque rupture and erosion leading to arterial thrombosis," Clin. Cardiol. **28**(9), 413–420 (2005).

40. T. Kume, T. Akasaka, T. Kawamoto, H. Okura, N. Watanabe, E. Toyota, Y. Neishi, R. Sukmawan, Y. Sadahira, and K. Yoshida, "Measurement of the thickness of the fibrous cap by optical coherence tomography," Am. Heart J. **152**(4), 755.e1–755.e4 (2006).

41. A. S. Kini, Y. Vengrenyuk, T. Yoshimura, M. Matsumura, J. Pena, U. Baber, P. Moreno, R. Mehran, A. Maehara, S. Sharma, and J. Narula, "Assessment of fibrous cap thickness by optical coherence tomography in vivo: reproducibility and standardization," J. Am. Coll. Cardiol. Published on-line, October 29, 2016.

42. D. L. Bhatt, *Cardiovascular Intervention: A Companion to Braunwald's Heart Disease* (Elsevier Health Sciences, 2015).

43. B. E. Bouma and G. J. Tearney, "Power-efficient nonreciprocal interferometer and linear-scanning fiber-optic catheter for optical coherence tomography," Opt. Lett. **24**(8), 531–533 (1999).

44. A. M. Rollins and J. A. Izatt, "Optimal interferometer designs for optical coherence tomography," Opt. Lett. **24**(21), 1484–1486 (1999).

45. G. J. Tearney, I. K. Jang, D. H. Kang, H. T. Aretz, S. L. Houser, T. J. Brady, K. Schlendorf, M. Shishkov, and B. E. Bouma, "Porcine coronary imaging in vivo by optical coherence tomography," Acta Cardiol. **55**(4), 233–237 (2000).

46. I.-K. Jang, G. Tearney, and B. Bouma, "Visualization of tissue prolapse between coronary stent struts by optical coherence tomography: comparison with intravascular ultrasound," Circulation **104**(22), 2754 (2001).

47. I. K. Jang, B. E. Bouma, D. H. Kang, S. J. Park, S. W. Park, K. B. Seung, K. B. Choi, M. Shishkov, K. Schlendorf, E. Pomerantsev, S. L. Houser, H. T. Aretz, and G. J. Tearney, "Visualization of coronary atherosclerotic plaques in patients using optical coherence tomography: comparison with intravascular ultrasound," J. Am. Coll. Cardiol. **39**(4), 604–609 (2002).

48. B. E. Bouma, G. J. Tearney, H. Yabushita, M. Shishkov, C. R. Kauffman, D. DeJoseph Gauthier, B. D. MacNeill, S. L. Houser, H. T. Aretz, E. F. Halpern, and I. K. Jang, "Evaluation of intracoronary stenting by intravascular optical coherence tomography," Heart **89**(3), 317–320 (2003).

49. P. Barlis, P. W. Serruys, N. Gonzalo, W. J. van der Giessen, P. J. de Jaegere, and E. Regar, "Assessment of culprit and remote coronary narrowings using optical coherence tomography with long-term outcomes," Am. J. Cardiol. **102**(4), 391–395 (2008).

50. I. K. Jang, G. J. Tearney, B. MacNeill, M. Takano, F. Moselewski, N. Iftima, M. Shishkov, S. Houser, H. T. Aretz, E. F. Halpern, and B. E. Bouma, "In vivo characterization of coronary atherosclerotic plaque by use of optical coherence tomography," Circulation **111**(12), 1551–1555 (2005).

51. T. Kubo, T. Imanishi, S. Takarada, A. Kuroi, S. Ueno, T. Yamano, T. Tanimoto, Y. Matsuo, T. Masho, H. Kitabata, K. Tsuda, Y. Tomobuchi, and T. Akasaka, "Assessment of culprit lesion morphology in acute myocardial infarction: ability of optical coherence tomography compared with intravascular ultrasound and coronary angioscopy," J. Am. Coll. Cardiol. **50**(10), 933–939 (2007).

52. O. C. Raffel, G. J. Tearney, D. D. Gauthier, E. F. Halpern, B. E. Bouma, and I. K. Jang, "Relationship between a systemic inflammatory marker, plaque inflammation, and plaque characteristics determined by intravascular optical coherence tomography," Arterioscler. Thromb. Vasc. Biol. **27**(8), 1820–1827 (2007).

53. S. Chia, O. Christopher Raffel, M. Takano, G. J. Tearney, B. E. Bouma, and I. K. Jang, "In-vivo comparison of coronary plaque characteristics using optical coherence tomography in women vs. men with acute coronary syndrome," Coron. Artery Dis. **18**(6), 423–427 (2007).

54. O. C. Raffel, J. C. Hannan, and I.-K. Jang, "Coronary stent malapposition as a result of a post-stenotic aneurysm detected by optical coherence tomography," J. Invasive Cardiol. **18**(11), 561–562 (2006).

55. E. Regar, J. Schaar, and P. W. Serruys, "Images in cardiology. Acute recoil in sirolimus eluting stent: real time, in vivo assessment with optical coherence tomography," Heart **92**(1), 123 (2006).

56. T. Sawada, J. Shite, T. Shinke, S. Watanabe, H. Otake, D. Matsumoto, Y. Imuro, D. Ogasawara, O. L. Paredes, and M. Yokoyama, "Persistent malapposition after implantation of sirolimus-eluting stent into intramural coronary hematoma: optical coherence tomography observations," Circ. J. **70**(11), 1515–1519 (2006).

57. M. Takano, I.-K. Jang, and K. Mizuno, "Neointimal proliferation around malapposed struts of a sirolimus-eluting stent: optical coherence tomography findings," Eur. Heart J. **27**(15), 1763 (2006).

58. P. Barlis, J. Tanigawa, and C. Di Mario, "Coronary bioabsorbable magnesium stent: 15-month intravascular ultrasound and optical coherence tomography findings," Eur. Heart J. **28**(19), 2319 (2007).

59. R. Gupta, O. C. Raffel, and I. K. Jang, "Severe intimal hyperplasia after sirolimus eluting stent deployment: evaluation by optical coherence tomography," **93**, Heart 754 (2007).

60. E. Regar, H. M. van Beusekom, W. J. van der Giessen, and P. W. Serruys, "Images in cardiovascular medicine. Optical coherence tomography findings at 5-year follow-up after coronary stent implantation," Circulation **112**(23), e345–e346 (2005).

61. M. Takano, S. Inami, I.-K. Jang, M. Yamamoto, D. Murakami, K. Seimiya, T. Ohba, and K. Mizuno, "Evaluation by optical coherence tomography of neointimal coverage of sirolimus-eluting stent three months after implantation," Am. J. Cardiol. **99**(8), 1033–1038 (2007).

62. J. Tanigawa, P. Barlis, and C. Di Mario, "Do unapposed stent struts endothelialise? In vivo demonstration with optical coherence tomography," Heart **93**(3), 378 (2007).

63. E. Camenzind, P. G. Steg, and W. Wijns, "Stent thrombosis late after implantation of first-generation drug-eluting stents: a cause for concern," Circulation **115**(11), 1440–1455, discussion 1455 (2007).

64. S. Waxman, I.-K. Jang, and J. F. Granada, (personal communication, 2004).

65. S. H. Yun, G. J. Tearney, B. J. Vakoc, M. Shishkov, W. Y. Oh, A. E. Desjardins, M. J. Suter, R. C. Chan, J. A. Evans, I. K. Jang, N. S. Nishioka, J. F. de Boer, B. E. Bouma, and B. E. Bouma, "Comprehensive volumetric optical microscopy in vivo," Nat. Med. **12**(12), 1429–1433 (2007).

66. E. A. Swanson and C. L. Petersen, "Methods and apparatus for high speed longitudinal scanning in imaging systems," US patent 6,191,862 (2001).

67. G. Häusler, (personal communication, 1998).

68. M. Wojtkowski, R. Leitgeb, A. Kowalczyk, T. Bajraszewski, and A. F. Fercher, "In vivo human retinal imaging by Fourier domain optical coherence tomography," J. Biomed. Opt. **7**(3), 457–463 (2002).

69. R. Leitgeb, C. Hitzenberger, and A. Fercher, "Performance of Fourier domain vs. time domain optical coherence tomography," Opt. Express **11**(8), 889–894 (2003).

70. J. F. de Boer, B. Cense, B. H. Park, M. C. Pierce, G. J. Tearney, and B. E. Bouma, "Improved signal-to-noise ratio in spectral-domain compared with time-domain optical coherence tomography," Opt. Lett. **28**(21), 2067–2069 (2003).

71. M. Choma, M. Sarunic, C. Yang, and J. Izatt, "Sensitivity advantage of swept source and Fourier domain optical coherence tomography," Opt. Express **11**(18), 2183–2189 (2003).

72. S. Yun, G. Tearney, J. de Boer, N. Iftimia, and B. Bouma, "High-speed optical frequency-domain imaging," Opt. Express **11**(22), 2953–2963 (2003).

73. S. H. Yun, G. Tearney, J. de Boer, and B. Bouma, "Motion artifacts in optical coherence tomography with frequency-domain ranging," Opt. Express **12**(13), 2977–2998 (2004).

74. W. Y. Oh, S. H. Yun, G. J. Tearney, and B. E. Bouma, "Wide tuning range wavelength-swept laser with two semiconductor optical amplifiers," IEEE Photonics Technol. Lett. **17**(3), 678–680 (2005).

75. W. Y. Oh, S. H. Yun, G. J. Tearney, and B. E. Bouma, "115 kHz tuning repetition rate ultrahigh-speed wavelength-swept semiconductor laser," Opt. Lett. **30**(23), 3159–3161 (2005).

76. S. H. Yun, C. Boudoux, G. J. Tearney, and B. E. Bouma, "High-speed wavelength-swept semiconductor laser with a polygon-scanner-based wavelength filter," Opt. Lett. **28**(20), 1981–1983 (2003).

77. S. H. Yun, C. Boudoux, M. C. Pierce, J. F. de Boer, G. J. Tearney, and B. E. Bouma, "Extended-cavity semiconductor wavelength-swept laser for biomedical imaging," IEEE Photonics Technol. Lett. **16**(1), 293–295 (2004).

78. R. Huber, M. Wojtkowski, and J. G. Fujimoto, "Fourier Domain Mode Locking (FDML): A new laser operating regime and applications for optical coherence tomography," Opt. Express **14**(8), 3225–3237 (2006).

79. M. Shishkov, B. E. Bouma, and G. J. Tearney, "System and method for optical coherence imaging," (Google Patents, 2008).

80. D. C. Adams, Y. Wang, L. P. Hariri, and M. J. Suter, "Advances in endoscopic optical coherence tomography catheter designs," IEEE J. Sel. Top. Quantum Electron. **22**(3), 1–12 (2016).

81. B. J. Vakoc, M. Shishko, S. H. Yun, W. Y. Oh, M. J. Suter, A. E. Desjardins, J. A. Evans, N. S. Nishioka, G. J. Tearney, and B. E. Bouma, "Comprehensive esophageal microscopy by using optical frequency-domain imaging (with video)," Gastrointest. Endosc. **65**(6), 898–905 (2007).

82. S. Yun, G. Tearney, J. de Boer, and B. Bouma, "Removing the depth-degeneracy in optical frequency domain imaging with frequency shifting," Opt. Express **12**(20), 4822–4828 (2004).

83. G. J. Tearney, S. Waxman, M. Shishkov, B. J. Vakoc, M. J. Suter, M. I. Freilich, A. E. Desjardins, W. Y. Oh, L. A. Bartlett, M. Rosenberg, and B. E. Bouma, "Three-dimensional coronary artery microscopy by intracoronary optical frequency domain imaging," JACC Cardiovasc. Imaging **1**(6), 752–761 (2008).

84. B. E. Bouma, S. H. Yun, B. J. Vakoc, M. J. Suter, and G. J. Tearney, "Fourier-domain optical coherence tomography: recent advances toward clinical utility," Curr. Opin. Biotechnol. **20**(1), 111–118 (2009).

85. S. J. Corbett, J. Cosgrave, G. Melzi, R. Babic, G. G. Biondi-Zoccai, C. Godino, N. Morici, F. Airoldi, I. Michev, M. Montorfano, G. M. Sangiorgi, E. Bonizzoni, and A. Colombo, "Patterns of restenosis after drug-eluting stent implantation: Insights from a contemporary and comparative analysis of sirolimus- and paclitaxel-eluting stents," Eur. Heart J. **27**(19), 2330–2337 (2006).

86. https://www.sjm.com

87. http://www.terumo-europe.com/en-emea/interventional-cardiology/imaging-products/console/lunawave%C2%AE-coronary-imaging-console

88. Y. Ino, T. Kubo, A. Tanaka, A. Kuroi, H. Tsujioka, H. Ikejima, K. Okouchi, M. Kashiwagi, S. Takarada, H. Kitabata, T. Tanimoto, K. Komukai, K. Ishibashi, K. Kimura, K. Hirata, M. Mizukoshi, T. Imanishi, and T. Akasaka, "Difference of culprit lesion morphologies between ST-segment elevation myocardial infarction and non-ST-segment elevation acute coronary syndrome: an optical coherence tomography study," JACC Cardiovasc. Interv. **4**(1), 76–82 (2011).

89. B. D. MacNeill, I. K. Jang, B. E. Bouma, N. Iftimia, M. Takano, H. Yabushita, M. Shishkov, C. R. Kauffman, S. L. Houser, H. T. Aretz, D. DeJoseph, E. F. Halpern, and G. J. Tearney, "Focal and multi-focal plaque macrophage distributions in patients with acute and stable presentations of coronary artery disease," J. Am. Coll. Cardiol. **44**(5), 972–979 (2004).

90. A. Tanaka, T. Imanishi, H. Kitabata, T. Kubo, S. Takarada, T. Tanimoto, A. Kuroi, H. Tsujioka, H. Ikejima, S. Ueno, H. Kataiwa, K. Okouchi, M. Kashiwaghi, H. Matsumoto, K. Takemoto, N. Nakamura, K. Hirata, M. Mizukoshi, and T. Akasaka, "Morphology of exertion-triggered plaque rupture in patients with acute coronary syndrome: an optical coherence tomography study," Circulation **118**(23), 2368–2373 (2008).

91. T. Tanimoto, T. Imanishi, A. Tanaka, T. Yamano, H. Kitabata, S. Takarada, T. Kubo, N. Nakamura, K. Hirata, M. Mizukoshi, and T. Akasaka, "Various types of plaque disruption in culprit coronary artery visualized by optical coherence tomography in a patient with unstable angina," Circ. J. **73**(1), 187–189 (2009).

92. J. Tian, J. Hou, L. Xing, S.-J. Kim, T. Yonetsu, K. Kato, H. Lee, S. Zhang, B. Yu, and I.-K. Jang, "Significance of intraplaque neovascularisation for vulnerability: optical coherence tomography study," Heart **98**(20), 1504–1509 (2012).

93. S. Uemura, K. Ishigami, T. Soeda, S. Okayama, J. H. Sung, H. Nakagawa, S. Somekawa, Y. Takeda, H. Kawata, M. Horii, and Y. Saito, "Thin-cap fibroatheroma and microchannel findings in optical coherence tomography correlate with subsequent progression of coronary atheromatous plaques," Eur. Heart J. **33**(1), 78–85 (2012).

94. A. Taruya, A. Tanaka, T. Nishiguchi, Y. Matsuo, Y. Ozaki, M. Kashiwagi, Y. Shiono, M. Orii, T. Yamano, Y. Ino, K. Hirata, T. Kubo, and T. Akasaka, "Vasa vasorum restructuring in human atherosclerotic plaque vulnerability: a clinical optical coherence tomography study," J. Am. Coll. Cardiol. **65**(23), 2469–2477 (2015).

95. F. Saia, K. Komukai, D. Capodanno, V. Sirbu, G. Musumeci, G. Boccuzzi, G. Tarantini, M. Fineschi, G. Tumminello, C. Bernelli, G. Niccoli, M. Coccato, B. Bordoni, H. Bezerra, G. Biondi-Zoccai, R. Virmani, and G. Guagliumi; OCTAVIA Investigators, "Eroded versus ruptured plaques at the culprit site of STEMI: in vivo pathophysiological features and response to primary PCI," JACC Cardiovasc. Imaging **8**(5), 566–575 (2015).

96. H. Jia, F. Abtahian, A. D. Aguirre, S. Lee, S. Chia, H. Lowe, K. Kato, T. Yonetsu, R. Vergallo, S. Hu, J. Tian, H. Lee, S. J. Park, Y. S. Jang, O. C. Raffel, K. Mizuno, S. Uemura, T. Itoh, T. Kakuta, S. Y. Choi, H. L. Dauerman, A. Prasad, C. Toma, I. McNulty, S. Zhang, B. Yu, V. Fuster, J. Narula, R. Virmani, and I. K. Jang, "In vivo diagnosis of plaque erosion and calcified nodule in patients with acute coronary syndrome by intravascular optical coherence tomography," J. Am. Coll. Cardiol. **62**(19), 1748–1758 (2013).

97. G. Guagliumi, V. Sirbu, G. Musumeci, R. Gerber, G. Biondi-Zoccai, H. Ikejima, E. Ladich, N. Lortkipanidze, A. Matiashvili, O. Valsecchi, R. Virmani, and G. W. Stone, "Examination of the in vivo mechanisms of late drug-eluting stent thrombosis: findings from optical coherence tomography and intravascular ultrasound imaging," JACC Cardiovasc. Interv. **5**(1), 12–20 (2012).

98. J.-S. Kim, I.-K. Jang, C. Fan, T. H. Kim, J.-S. Kim, S. M. Park, E.-Y. Choi, S. H. Lee, Y.-G. Ko, D. Choi, M. K. Hong, and Y. Jang, "Evaluation in 3 months duration of neointimal coverage after zotarolimus-eluting stent implantation by optical coherence tomography: the ENDEAVOR OCT trial," JACC Cardiovasc. Interv. **2**(12), 1240–1247 (2009).

99. Z. A. Ali, A. Maehara, P. Généreux, R. A. Shlofmitz, F. Fabbiocchi, T. M. Nazif, G. Guagliumi, P. M. Meraj, F. Alfonso, H. Samady, T. Akasaka, E. B. Carlson, M. A. Leesar, M. Matsumura, M. O. Ozan, G. S. Mintz, O. Ben-Yehuda, and G. W. Stone; ILUMIEN III: OPTIMIZE PCI Investigators, "Optical coherence tomography compared with intravascular ultrasound and with angiography to guide coronary stent implantation (ILUMIEN III: OPTIMIZE PCI): a randomised controlled trial," Lancet **388**(10060), 2618–2628 (2016).

100. N. Meneveau, G. Souteyrand, P. Motreff, C. Caussin, N. Amabile, P. Ohlmann, O. Morel, Y. Lefrançois, V. Descotes-Genon, J. Silvain, N. Braik, R. Chopard, M. Chatot, F. Ecarnot, H. Tauzin, E. Van Belle, L. Belle, and F. Schiele, "Optical coherence tomography to optimize results of percutaneous coronary intervention in patients with non–ST-elevation acute coronary syndrome: clinical perspective," Circulation **134**(13), 906–917 (2016).

101. T. Soeda, S. Uemura, S.-J. Park, Y. Jang, S. Lee, J.-M. Cho, S.-J. Kim, R. Vergallo, Y. Minami, D. S. Ong, L. Gao, H. Lee, S. Zhang, B. Yu, Y. Saito, and I. K. Jang, "Incidence and clinical significance of poststent optical coherence tomography findings one-year follow-up study from a multicenter registry," Circulation **132**(11), 1020–1029 (2015).

102. M. Sabaté, S. Windecker, A. Iñiguez, A. Okkels-Jensen, A. Cequier, S. Brugaletta, S. H. Hofma, L. Räber, E. H. Christiansen, M. Suttorp, T. Pilgrim, G. Anne van Es, Y. Sotomi, H. M. García-García, Y. Onuma, and P. W. Serruys, "Everolimus-eluting bioresorbable stent vs. durable polymer everolimus-eluting metallic stent in patients with ST-segment elevation myocardial infarction: results of the randomized ABSORB ST-segment elevation myocardial infarction-TROFI II trial," Eur. Heart J. **37**(3), 229–240 (2016).

103. A. König, M. P. Margolis, R. Virmani, D. Holmes, and V. Klauss, "Technology insight: in vivo coronary plaque classification by intravascular ultrasonography radiofrequency analysis," Nat. Clin. Pract. Cardiovasc. Med. **5**(4), 219–229 (2008).

104. N. Uribe-Patarroyo and B. E. Bouma, "Rotational distortion correction in endoscopic optical coherence tomography based on speckle decorrelation," Opt. Lett. **40**(23), 5518–5521 (2015).

105. T. Wang, T. Pfeiffer, E. Regar, W. Wieser, H. van Beusekom, C. T. Lancee, G. Springeling, I. Krabbendam, A. F. van der Steen, R. Huber, and G. van Soest, "Heartbeat OCT: in vivo intravascular megahertz-optical coherence tomography," Biomed. Opt. Express **6**(12), 5021–5032 (2015).

106. T. S. Kim, H.-S. Park, S.-J. Jang, J. W. Song, H. S. Cho, S. Kim, B. E. Bouma, J. W. Kim, and W.-Y. Oh, "Single cardiac cycle three-dimensional intracoronary optical coherence tomography," Biomed. Opt. Express **7**(12), 4847–4858 (2016).

107. M. Villiger, E. Z. Zhang, S. Nadkarni, W. Y. Oh, B. E. Bouma, and B. J. Vakoc, "Artifacts in polarization-sensitive optical coherence tomography caused by polarization mode dispersion," Opt. Lett. **38**(6), 923–925 (2013).

108. E. Z. Zhang, W. Y. Oh, M. L. Villiger, L. Chen, B. E. Bouma, and B. J. Vakoc, "Numerical compensation of system polarization mode dispersion in polarization-sensitive optical coherence tomography," Opt. Express **21**(1), 1163–1180 (2013).

109. M. Villiger, E. Z. Zhang, S. K. Nadkarni, W. Y. Oh, B. J. Vakoc, and B. E. Bouma, "Spectral binning for mitigation of polarization mode dispersion artifacts in catheter-based optical frequency domain imaging," Opt. Express **21**(14), 16353–16369 (2013).
110. N. Lippok, M. Villiger, and B. E. Bouma, "Degree of polarization (uniformity) and depolarization index: unambiguous depolarization contrast for optical coherence tomography," Opt. Lett. **40**(17), 3954–3957 (2015).
111. K. Fujii, H. Hao, M. Shibuya, T. Imanaka, M. Fukunaga, K. Miki, H. Tamaru, H. Sawada, Y. Naito, M. Ohyanagi, S. Hirota, and T. Masuyama, "Accuracy of OCT, grayscale IVUS, and their combination for the diagnosis of coronary TCFA: an ex vivo validation study," JACC Cardiovasc. Imaging **8**(4), 451–460 (2015).
112. J. Li, X. Li, D. Mohar, A. Raney, J. Jing, J. Zhang, A. Johnston, S. Liang, T. Ma, K. K. Shung, S. Mahon, M. Brenner, J. Narula, Q. Zhou, P. M. Patel, and Z. Chen, "Integrated IVUS-OCT for real-time imaging of coronary atherosclerosis," JACC Cardiovasc. Imaging **7**(1), 101–103 (2014).
113. N. Uribe-Patarroyo, M. Villiger, and B. E. Bouma, "Quantitative technique for robust and noise-tolerant speed measurements based on speckle decorrelation in optical coherence tomography," Opt. Express **22**(20), 24411–24429 (2014).
114. N. Uribe-Patarroyo and B. E. Bouma, "Velocity gradients in spatially resolved laser Doppler flowmetry and dynamic light scattering with confocal and coherence gating," Phys. Rev. E Stat. Nonlin. Soft Matter Phys. **94**(2-1), 022604 (2016).
115. T.-H. Tsai, O. O. Ahsen, H.-C. Lee, K. Liang, M. Figueiredo, Y. K. Tao, M. G. Giacomelli, B. M. Potsaid, V. Jayaraman, Q. Huang, A. E. Cable, J. G. Fujimoto, and H. Mashimo, "Endoscopic optical coherence angiography enables 3-dimensional visualization of subsurface microvasculature," Gastroenterology **147**(6), 1219–1221 (2014).
116. C. P. Fleming, H. Wang, K. J. Quan, and A. M. Rollins, "Real-time monitoring of cardiac radio-frequency ablation lesion formation using an optical coherence tomography forward-imaging catheter," J. Biomed. Opt. **15**(3), 030516 (2010).
117. H. W. Baac, N. Uribe-Patarroyo, and B. E. Bouma, "High-energy pulsed Raman fiber laser for biological tissue coagulation," Opt. Express **22**(6), 7113–7123 (2014).
118. K. Beaudette, H. W. Baac, W. J. Madore, M. Villiger, N. Godbout, B. E. Bouma, and C. Boudoux, "Laser tissue coagulation and concurrent optical coherence tomography through a double-clad fiber coupler," Biomed. Opt. Express **6**(4), 1293–1303 (2015).
119. J. Kim, A. Ahmad, J. Li, M. Marjanovic, E. J. Chaney, K. S. Suslick, and S. A. Boppart, "Intravascular magnetomotive optical coherence tomography of targeted early-stage atherosclerotic changes in ex vivo hyperlipidemic rabbit aortas," J. Biophotonics **9**(1-2), 109–116 (2016).
120. H. Yoo, J. W. Kim, M. Shishkov, E. Namati, T. Morse, R. Shubochkin, J. R. McCarthy, V. Ntziachristos, B. E. Bouma, F. A. Jaffer, and G. J. Tearney, "Intra-arterial catheter for simultaneous microstructural and molecular imaging in vivo," Nat. Med. **17**(12), 1680–1684 (2011).
121. S. Kim, M. W. Lee, T. S. Kim, J. W. Song, H. S. Nam, H. S. Cho, S.-J. Jang, J. Ryu, D. J. Oh, D.-G. Gweon, S. H. Park, K. Park, W. Y. Oh, H. Yoo, and J. W. Kim, "Intracoronary dual-modal optical coherence tomography-near-infrared fluorescence structural-molecular imaging with a clinical dose of indocyanine green for the assessment of high-risk plaques and stent-associated inflammation in a beating coronary artery," Eur. Heart J. **37**(37), 2833–2844 (2016).
122. G. J. Ughi, H. Wang, E. Gerbaud, J. A. Gardecki, A. M. Fard, E. Hamidi, P. Vacas-Jacques, M. Rosenberg, F. A. Jaffer, and G. J. Tearney, "Clinical characterization of coronary atherosclerosis with dual-modality OCT and near-infrared autofluorescence imaging," JACC Cardiovasc. Imaging **9**(11), 1304–1314 (2016).
123. J. W. Verjans, E. A. Osborn, G. J. Ughi, M. A. Calfon Press, E. Hamidi, A. P. Antoniadis, M. I. Papafaklis, M. F. Conrad, P. Libby, P. H. Stone, R. P. Cambria, G. J. Tearney, and F. A. Jaffer, "Targeted near-infrared fluorescence imaging of atherosclerosis," JACC Cardiovasc. Imaging **9**(9), 1087–1095 (2016).
124. C. V. Bourantas, F. A. Jaffer, F. J. Gijsen, G. van Soest, S. P. Madden, B. K. Courtney, A. M. Fard, E. Tenekecioglu, Y. Zeng, A. F. W. van der Steen, S. Emelianov, J. Muller, P. H. Stone, L. Marcu, G. J. Tearney, and P. W. Serruys, "Hybrid intravascular imaging: recent advances, technical considerations, and current applications in the study of plaque pathophysiology," Eur. Heart J. **38**(6), 400–412 (2017).

1. Introduction

The first biomedical application of optical coherence tomography (OCT) was the visualization of the microstructure of the retina [1,2]. In some respects, the eye represents an ideal sample for examination using optical methods. The anterior segment, vitreous and even the superficial retina are highly transparent, exhibit low scattering, and are directly accessible for imaging. Applying OCT, instead, to more turbid and less accessible tissues required substantial modification of the technology, including the development of minimally invasive catheters and rotational couplers, the use of longer wavelength sources for improved imaging depth, and the increase of imaging speed to achieve high quality images despite the significant motion that can be present in many organ systems. Many compelling diagnostic and interventional clinical applications motivated solutions to these technical limitations through

engineering innovations that have shaped catheter-based OCT as a novel method for cross-sectional imaging *in vivo* with resolution approaching that of histology [3]. Intravascular imaging, in particular, was one of the earliest goals.

Rupture or erosion of a coronary atherosclerotic plaque is the most common cause of acute myocardial infarction (AMI), the leading cause of death in the United States and industrialized countries [4]. Atherosclerotic plaques are composed of fibrous tissue and lipid-rich regions. When lipid pools are present within a plaque, they are typically separated from the vascular lumen by a fibrous cap that varies greatly in thickness, strength, stiffness, and cellularity. Lipid-rich regions are soft and impart stress to the fibrous cap, thus making the plaque prone to rupture [5, 6]. The fibrous cap can contain numerous activated inflammatory macrophages. Enzymes secreted by activated macrophages, such as matrix metalloproteinases, MMP-1 and MMP-13, can degrade the fibrous component resulting in thin caps with less structural integrity at these locations [5–7]. Early retrospective autopsy studies showed that the three most important characteristics of vulnerable coronary plaques were 1) thin fibrous caps (<65 μm), 2) the presence and composition of lipid pools, and 3) activated macrophages near the fibrous cap [5, 6, 8]. While plaques with large lipid pools and thin fibrous caps comprised approximately 60% of plaques that had caused an acute event, further autopsy studies revealed that coronary plaques with surface erosions were also associated with acute thrombosis and sudden occlusion of coronary arteries [8].

A method capable of identifying vulnerable coronary plaques prior to rupture was already a prominent objective in the 1990s, primarily as a means to develop a therapeutic strategy specifically designed for a given patient. For example, in patients with isolated vulnerable plaques in the proximal coronary artery, local treatments such as balloon angioplasty, stenting, local delivery therapy, or radiation brachytherapy were of interest to prevent acute coronary syndromes [9,10]. Imaging technologies that existed prior to OCT included intravascular ultrasound (IVUS), magnetic resonance imaging (MRI), and computed tomography (CT). IVUS was widely available for use in interventional cardiology to obtain local structure including reference vessel diameter and localization of calcium, and to confirm stent deployment. However, the relatively low resolution of IVUS (~100 μm at 40 MHz) prevented visualization of the fine structures of plaques such as macrophages and thin fibrous caps [11, 12]. MRI had a resolution similar to that of IVUS (~100 μm), and was likewise inadequate to discriminate fine scale plaque features [13, 14]. In the 1990s, coronary artery calcification (CAC) score was examined to estimate the atherosclerotic burden by electron beam or multislice computed tomography (CT). Measurements of CAC score, as quantified by CT, were shown to predict future cardiovascular events [15]. The first use of contrast-enhanced CT to obtain noninvasive coronary angiograms was in 1995 [16, 17], however, the detection of vulnerable plaques prone to rupture on the basis of coronary CT remained challenging. Experimental intravascular methods such as angioscopy had also been proposed to determine plaque vulnerability. Preliminary studies suggested that plaques with a glistening yellow surface, seen by angioscopic examination, were correlated with acute events [18]. However, angioscopy only allowed visualization of the surface of plaques and additionally required extended periods of blood flow occlusion, which carried risk of ischemia.

In addition to the imaging specifications for intravascular OCT that derived from the specific diagnostic objectives discussed above, intravascular OCT would be deployed in the cardiac catheterization laboratory, which placed further constraints on engineering specifications. The "cath lab" has specialized equipment that permits testing and imaging of cardiac function. Procedures begin with the insertion of a narrow diameter plastic tube or guide catheter into the radial artery of the arm or into the femoral artery in the groin. By placing the distal tip of the guide catheter at the entrance to each main coronary artery and injecting radiopaque dye, an X-ray movie (angiogram) can be acquired to visualize the outline of the coronaries and identify stenoses or blockages. In the event of severe stenosis, a fine flexible wire, typically 0.3 mm in diameter and termed a guide wire, can be inserted through the guide catheter

and into the coronary artery. Additional devices for inspecting or treating coronary disease are threaded onto this wire for deployment into the coronary. An OCT imaging catheter must therefore have a narrow diameter, sufficient length, and the right amount of flexibility while preserving "pushability" for insertion over the guide wire and within the guide catheter. Additionally, intravascular instruments must be "atraumatic" to avoid damaging the delicate arterial endothelium. Since diagnostic catheterization is performed in over 1 million patients per year in the US [4], practical catheter devices must be inexpensive and easy to manufacture in large quantities if used in routine clinical practice.

2. Catheter-based time domain OCT

The initial efforts to address the technical barriers inhibiting OCT from applications in biological tissues outside of the structures of the eye began in 1993. Originally, OCT was performed in the time domain, using a broad wavelength band source, and axially moving the reference mirror to scan the coherence gate across the sample depth. Over the following few years, solutions were found that permitted the demonstration of catheter-based time domain OCT in rabbits *in vivo* and in human tissues *ex vivo*.

2.1 Catheters

OCT imaging of blood vessels most conveniently exploits the cylindrical morphology by collecting signals along the radial coordinate through interferometry and then scanning the angular coordinate by rotation as the fastest mechanical scan priority. The third, longitudinal dimension is then scanned as the slowest priority through pullback actuation. This paradigm requires a catheter capable of emitting a focused beam transverse to its longitudinal axis. As in most applications, the optimal focal spot size is determined as a compromise between resolution and depth of field, and typically focal sizes on the order of 25 μm meet this consideration. While human vessels can span a wide range of lumen diameters, coronary arteries are typically a few millimeters in diameter, suggesting that a catheter focal distance of roughly 2 mm is an appropriate optical design target.

The first imaging catheters (Fig. 1(B), 1(C)) that were made for OCT were based on single mode fiber and the combination of a 0.7 mm diameter gradient index lens, polished to the appropriate length (0.2725 pitch), and a 0.5 mm prism for angularly deflecting the beam [19–21].

2.2 Rotary junction

Actuating the distal rotational scan in a catheter was initially accomplished by embedding the optical fiber of the catheter within a flexible torque cable and connecting the proximal end to a rotational coupler or 'rotary junction'. The prototype OCT rotary junction (Fig. 1(D)) was configured using optical ferrules that were placed within a mating sleeve in butt-coupling contact [19]. One ferrule, which was fixed and not allowed to rotate, was in optical connection with the OCT interferometer. The second ferrule, which was free to rotate, was connected to the optical fiber of the catheter. A motor was then used to rotate the catheter while maintaining optical connection within the mating sleeve. In order to reduce back reflections and also to lubricate the ferrule interface, index matching oil was inserted between the optical faces. Single pass insertion loss of this prototype, averaged over one rotation, was 5 dB with a 6 dB (max to min) variation. Despite the very slow rotational speed, which ranged from 1 to 12 RPM, the optical connectors degraded rapidly, increasing the insertion loss and decreasing the return loss.

2.3 Light source

The first OCT systems used near infrared light of roughly 800 nm wavelength [2, 22], which propagated well through the anterior eye and vitreous, permitting imaging of the thin retinal membrane. Most other tissues of the human body, however, have significant attenuation in

this spectral band, primarily mediated by scattering. The rapid decrease in scattering with increasing wavelength motivated investigating the use of infrared light. A comparison of OCT imaging in human cadaveric specimens [23] with wavelengths of 830 nm, 1.3 µm, 1.55 µm, and 1.8 µm showed a marked increase in depth of penetration for the infrared and concentrated source development efforts on the 1.25 µm to 1.35 µm range. Although InGaAs photodetectors were available for this spectrum, low coherence sources were very limited. One early source [24] was constructed from a solid-state gain medium, chromium forsterite (Cr^{4+}:Mg_2SiO_4) [25]. In order to enhance OCT resolution, the ultrafast pulses emitted from the laser were spectrally broadened through self-phase modulation in a small core optical fiber [24]. This laser provided 6 µm axial resolution and ample average power. Since the pulse repetition rate was far faster then the integration time of the digital acquisition of the OCT interferogram, the laser was effectively continuous wave.
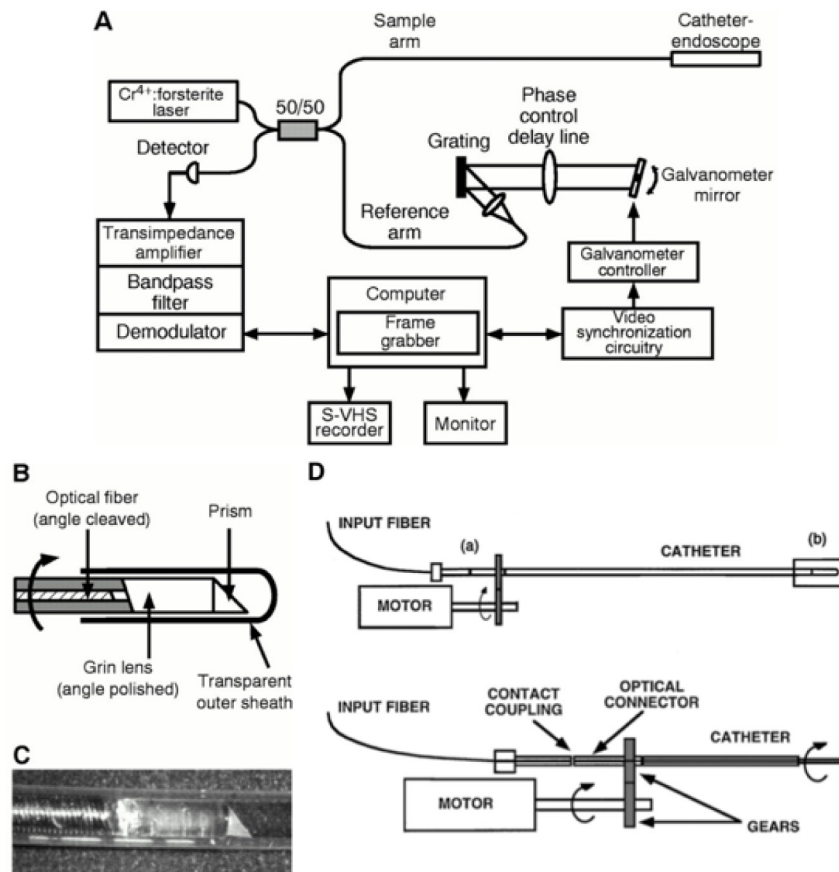
Fig. 1. First catheter-based time domain OCT system (A), catheter (B, C), and rotary junction (D). Reprinted from [19], and [29] with permission from Elsevier.

2.4 Delay scanning

First generation OCT systems utilized mechanical delay scanning, typically based on a galvanometer to drive an arm upon which a retroreflector had been mounted. These devices were mechanically limited to scans of a few millimeters and something on the order of 100 Hz scanning repetition rate. For a conventional image comprising 500 A-lines per rotation, this speed was too slow to avoid the significant motion artifacts that arise due to heart motion. An alternative approach was derived from a group velocity scanner used for autocorrelation measurements of ultrafast laser pulses [26]. When applied to OCT, this configuration had the

unique capability of independently controlling the phase delay rate and the group delay rate [27]. This allowed the carrier frequency in OCT to be adjusted independently from the scanning range and rate and provided a scanning repetition rate of up to 4 kHz [27, 28].

2.5 System integration

Since the objective for the first catheter-based system was to test early concepts, no effort was made to make the system portable. Indeed, the system comprised an extensive apparatus that was arrayed across two 4' x 8' optical tables and, primarily due to the complicated laser, was very environmentally unstable. Nevertheless, the system was capable of 10 μm axial resolution and yielded a detection sensitivity of 110 dB neglecting losses in the rotary junction. Although the axial scanning repetition rate was 1 kHz, the image acquisition speed was just 1 frame per five seconds due to the rotary junction limitations. Although the catheter used in these studies had an outside diameter of only 1 mm, its flexibility was insufficient to support use for intravascular imaging *in vivo* in the rabbit and the first publication of its use demonstrated im aging of the gastrointestinal tract and trachea (Fig. 2) [29]. Not long after this result, in 1999, the first intravascular imaging was reported in a study that demonstrated imaging of the rabbit abdominal aorta [30]. In order to overcome the attenuation of scattering by blood, this study infused saline directly into the aorta.
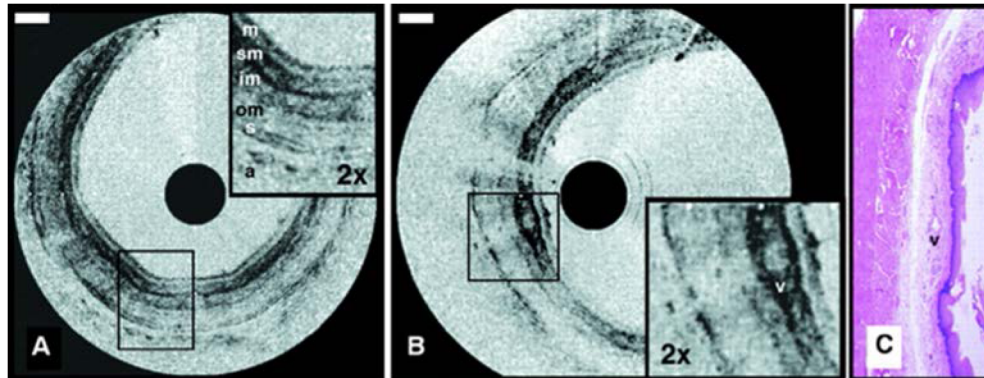

Fig. 2. Images obtained using the first catheter-based time domain OCT system for visualizing the rabbit esophagus *in vivo* displayed in inverse gray scale. Esophageal layers can be clearly delineated: mucosa (m); submucosa (sm); inner and outer muscularis (im and om); serosa (s). A vessel (v) in the submucosa can also be seen. Reprinted from [29] with permission from Elsevier.

3. Image interpretation criteria

In order to understand the potential of OCT for imaging the structure of coronary arteries, initial studies isolated human cadaver coronaries and drew comparisons between the OCT findings and histopathology [3, 20], demonstrating the ability to delineate the tri-laminar, intima-media-adventitia, structure of coronaries. Subsequent studies, including those conducted with Fourier domain OCT, advanced image interpretation criteria significantly based on more than 350 correlated OCT image – histology pairs from nearly 100 cadavers and representing a spectrum of atherosclerotic disease [31]. The primary findings of this work are summarized in Table 1. Specifically, normal vessels are characterized by three uniform layers: a high reflectance, thin, inner band corresponding to the intima, a lower signal second band, corresponding to the media, and a return to higher reflection in the outer band, corresponding to the adventitia. Depending on the use of a regular or inverse gray scale for tomogram display, a higher reflection signal corresponds to a brighter (normal), or darker (inverse) pixel value. In contrast, plaques either obliterate the layered structure altogether or, at a minimum, significantly expand the innermost layer. Plaques having a dominant content of fibrous tissue exhibit a uniform, homogeneous high scattering signal. Both lipid rich plaques and cal-

cific plaques are characterized by a signal-poor, or echolucent, zone and can be distinguished from each other based on the borders of this zone: lipid rich plaques have diffuse borders with a very rapid signal decay while calcific plaques have a very sharp echolucent zone and good signal penetration. Based on these simple and easily applied visual criteria, the sensitivity and specificity for classifying plaques in this simplified scheme were 75% and 97% for fibrous plaques, 95% and 97% for calcific plaques, and 92% and 91% for lipid-rich plaques.

Table 1. OCT Image Interpretation Criteria for Vascular Features

Arterial / Plaque Feature	Image Interpretation Criteria
Normal Vessel	Three concentric layers: high/low/high scattering [31]
Fibrous Plaque	Homogenous high scattering [31]
Calcific Nodule	Echolucent, sharp borders, high penetration [31]
Lipid Rich (Atheroma)	Echolucent, diffuse borders, high attenuation [31]
Macrophages	Punctate signal, high standard deviation [32, 33]
Cholesterol Crystals	Very high scattering, linear structures [34, 35]
Collagen / Smooth Muscle	Birefringent [36–38]
Acute (Red) Thrombus	Low birefringence, high attenuation [37, 38]
Chronic (White) Throm-	High birefringence, low attenuation [37, 38]

Additional autopsy studies investigated image interpretation criteria for further plaque features. Given the very important role that macrophages play in atherogenesis, plaque progression, and collagen degeneration, methods for identifying them based on OCT were an important early advancement [33]. Based on the insight that lipid-laden phagolysosomes in macrophages have a size comparable with infrared wavelengths and a high contrast of index of refraction in comparison with the cytoplasm, this early work hypothesized that macrophages should give rise to a punctate OCT signal characterized by a high standard deviation. Indeed, this metric was shown to correlate well (r = 0.84) with CD68 immunohistochemical staining for macrophages. This work has been reinforced by numerous subsequent studies, most recently by a study that independently confirmed the high sensitivity (100%) and specificity (96.8%) for identifying regions of elevated macrophage concentration [32]. Perhaps a more subtle but intriguing finding of autopsy vessel studies indicated that OCT may be able to identify cholesterol crystals [34]. This finding is important in light of the possible role that cholesterol crystals may play in disrupting vulnerable plaques [39].

Another plaque metric that is considered to be highly relevant for determining stability against disruption and thrombotic occlusion is the thickness of the fibrotic tissue or 'cap' overlying lipid rich plaques. Autopsy studies have suggested that caps below 65 µm are particularly disposed to mechanical disruption [8]. While early studies indicated that OCT was suitable for cap thickness measurement [31, 33], more recently, careful examination has demonstrated excellent correlation (r = 0.90) and agreement (mean difference in Bland-Altman analysis of −24 µm) between OCT and histological measurement of cap thickness [40, 41].
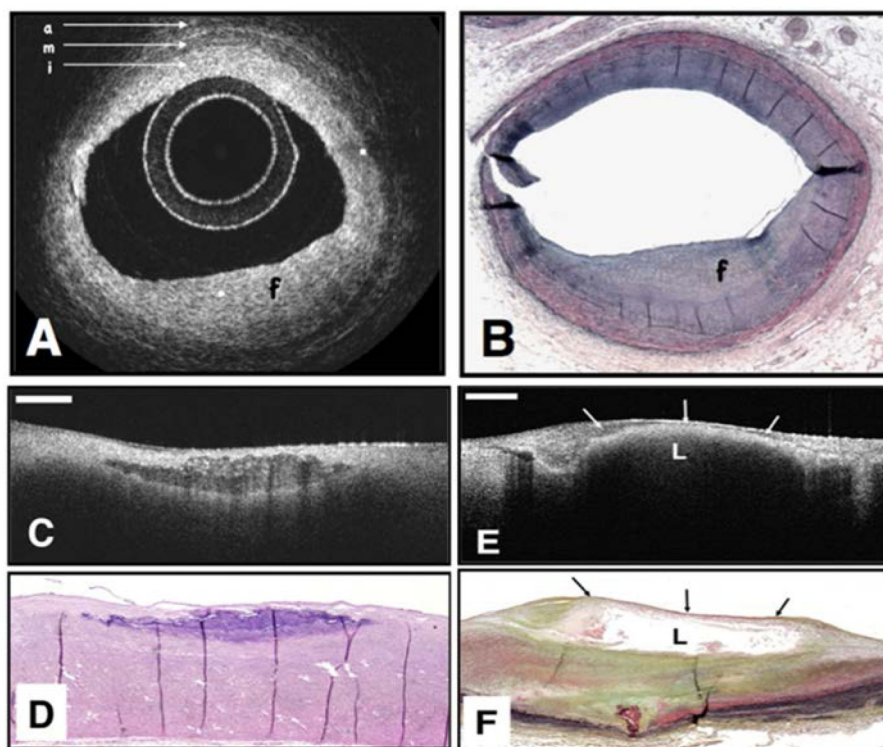
Fig. 3. OCT image (A) of a fibrous coronary plaque showing a homogeneous, signal-rich interior (f) as well as the three-layered structure of intima (i), media (m), adventitia (a). Corresponding histology (B). OCT image of fibrocalcific aortic plaque (C) showing a sharply delineated region with a signal-poor interior. Corresponding histology (D). OCT image of a lipid-rich plaque (E) showing signal-poor region (L) with poorly delineated borders. Corresponding histology (F). Reprinted from [31].

While macrophages, cholesterol crystals and thin fibrous caps are thought to be associated with plaque instability, collagen and smooth muscle impart mechanical integrity to plaques and there is great current interest in methods to increase these components through new drugs. The ability of OCT to map collagen and smooth muscle was first demonstrated in 2007 based on measurements of birefringence by polarization-sensitive (PS) OCT [36]. This first work compared the slope of the accumulated phase retardation over depth of penetration with collagen and smooth muscle as identified by histology and found a statistically significant positive correlation (r = 0.67) between this metric and total collagen content, thick collagen fiber content (r = 0.76), and smooth muscle density (r = 0.74). Although this work utilized time-domain OCT and a microscope scanner with open, prepared aorta cadaver samples, it stimulated significant later work to extend the capabilities of PS imaging for coronary imaging *in vivo*. This later work will be discussed in Section 8.

4. First-in-man studies with time domain intravascular OCT

Motivated by the results from the initial studies imaging cadaver coronary arteries, significant effort was directed toward the development of a clinically viable imaging system and catheter. Without preliminary imaging results from living human subjects, it was difficult to justify the significant expense required to develop a commercial system and production capacity for disposable intracoronary catheters. In comparison, the development of a system and catheter within the academic sector proved to be faster and more efficient. This section describes the specific engineering advances that were undertaken, beginning in early 1998, in order to facil-

itate clinical translation into a pilot human subject study and the results from the first-in-man trial.

4.1 Catheters

Intravascular catheters must be inserted through a guide catheter, an open-lumen tube having an inner diameter of roughly 2 mm, that secures access to the entrance or ostium of the coronary of interest. Further guidance as the imaging catheter is advanced into the coronary is provided by the guide wire, typically of 0.014 inches in diameter, which is positioned under fluoroscopic guidance in advance of the imaging procedure [42]. At the distal tip of the imaging catheter, there is a guide wire provision that permits the wire to be threaded through the tip and then to exit the lumen 1-2 cm proximal so that the catheter is guided in parallel to the guide wire.

Compatibility of the imaging catheter with the guide catheter and guide wire, requires that it has a length over 1.5 m and a diameter less than roughly 1 mm. In addition, the distal ~10 cm must be very flexible and atraumatic while the proximal remainder ideally will have a progressively (moving proximally) increasing stiffness so that the catheter can be pushed through the guide catheter along its entire length. Additionally, the catheter must be biocompatible and sterile.

IVUS catheters, which were introduced roughly a decade before intravascular OCT, were relatively mature by 1998 and met the mechanical and biocompatibility requirements with a design based on an external, plastic sheath and an internal torque cable [12]. The sheath was designed to ensure the appropriate proximal stiffness and distal flexibility while the torque cable housed the twisted wire pair for transducing the RF signals to/from the distal piezoelectric element. Constructing the first OCT catheters was achieved by disassembling commercial IVUS catheters and utilizing the sheaths and torque cables [43]. Since OCT does not require a specific transducing medium as does IVUS, the distal flushing port in the IVUS sheaths was closed using a biocompatible adhesive. The IVUS torque cables were modified by removing the twisted wire pair and piezoelectric transducer and replacing them with optical fiber and a distal gradient index lens and prism. Following reassembly, the OCT catheters were sterilized with a conventional cold ethylene oxide process.

4.2 Rotary junction

In the cardiac catheterization laboratory, IVUS is commonly performed by placing the rotary junction in a sterile bag so that it can be connected directly to the catheter at the vascular access point. Although the design of the prototype OCT rotary junction was facilitated by butt coupling through optical connectors, the approach was impractical for faster rotation and robust operation. Rotary junctions commercially available at this time suffered from high backreflection, frustrating their use for OCT imaging. Instead, a rotary junction was developed that physically separated the motor from the optical rotational joint. The latter was formed by placing one aspheric collimating lens in a rotor and a second, matching, aspheric lens in a stator. Within the rotor, a single-mode optical fiber was fixed with respect to the lens and connectorized at the opposing end to permit connection to an OCT catheter. A second optical fiber was mounted within the stator and used to connect the rotary junction to the OCT system. The lenses of the optical rotary junction were precisely aligned to minimize insertion loss from fiber input to fiber output and were epoxy bonded in place following alignment. Within the rotary junction, an electric motor was mounted with its rotor axis parallel to that of the optical unit and the two were connected by a cogged belt (Fig. 4), permitting rotational speeds of 200-300 RPM. The final unit had less than 1 dB single pass insertion loss and less than 0.4 dB variation of insertion loss with rotation.
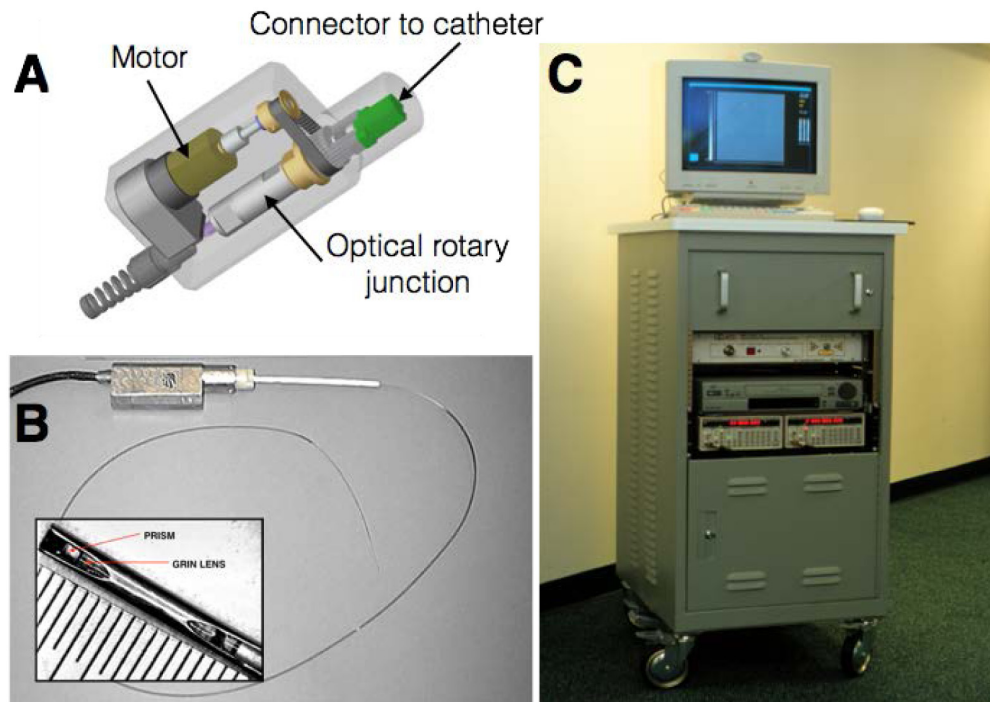
Fig. 4. Mechanical schematic (A) and photograph (B) of first clinically-viable OCT catheter and rotary junction. The catheter was configured to be connected to the portable time-domain OCT console (C).

4.3 Light source

Perhaps the most profound engineering step that was required to move from the first laboratory-based intravascular OCT system to a configuration suitable for use in the human cardiac catheterization unit was revising the light source. While the original modelocked $Cr:Mg_2SiO_4$ laser provided high power and large bandwidth, it was far too large and environmentally unstable to be practical. Fortunately, in the late 1990s, the optical telecommunications industry was expanding and focusing interest on 'fiber to the home' technologies. This effort led to the development, by Philips Research in Eindhoven, to a multiple quantum well semiconductor optical amplifier (SOA) that provided polarization independent gain near 1.3 microns. When this SOA was configured as an amplified spontaneous emission source, it emitted several milliwatts of continuous wave power having a nearly Gaussian spectrum spanning approximately 80 nm. In comparison with the modelocked laser source, the power provided by the SOA was quite low, motivating the development of new interferometer designs that improved optical efficiency and compensated for detection sensitivity penalties [43, 44].

It is interesting to note that during the years preceding the burst of the 'telecom bubble' in 2001, an enormous industry investment led directly to several important technologies, such as the 1.3 μm SOA, fiber optic circulators and splitters, that enabled OCT research and development at a cost that never would have been supported by medical device research budgets.
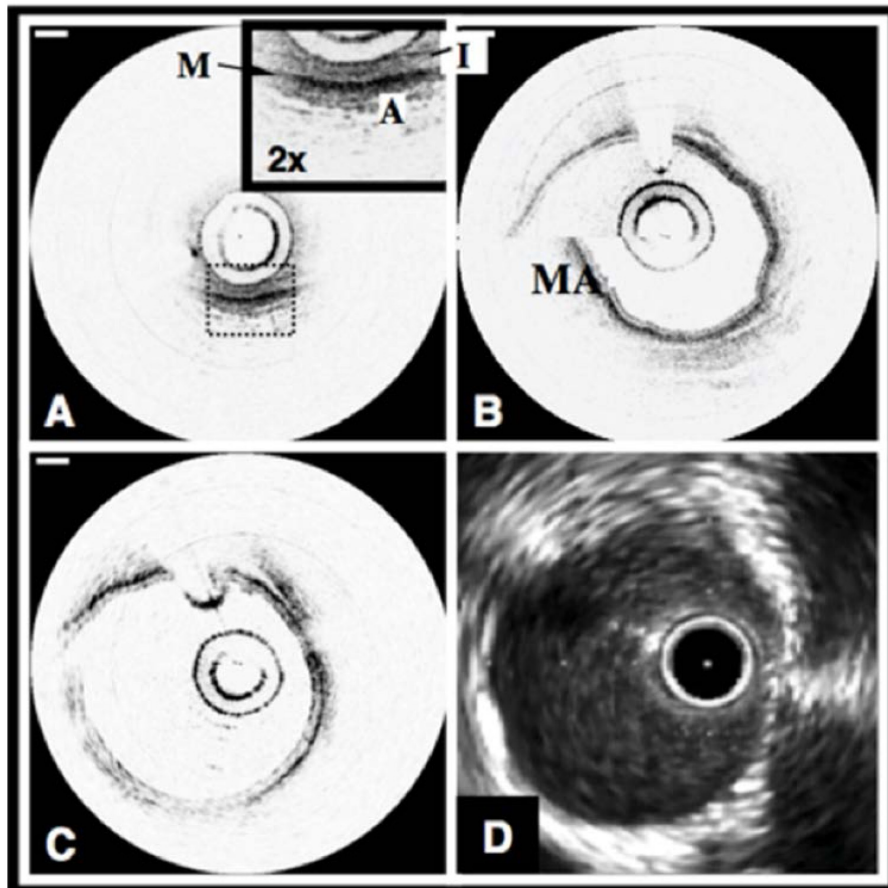
4.4 Clinical translation

Fig. 5. Normal swine coronary arteries. A. OCT image of the circumflex coronary artery acquired at 4 fps without a saline purge. The layers of the artery, the intima (I), media (M), and adventitia (A) can be clearly identified. B. OCT image of the right coronary artery acquired at 4 fps with a selective saline flush. The motion artifact (MA) is a misregistration of the image through one catheter rotation. C. OCT image acquired at 8 fps. D. IVUS image of the coronary artery in Fig. 1(C). OCT scale bars, 500 μm, IVUS tick marks, 1 mm. OCT displayed in inverse gray scale. Reprinted from [45].

In addition to the more important alterations of the catheters, rotary junction and light source, clinical viability also required packaging the entire OCT system in a robust, portable cart suitable for transportation to and operation in the cardiac catheterization laboratory (Fig. 4(C)). Initial evaluation of the imaging performance and safety of the complete system was conducted in swine coronary arteries *in vivo* [45]. Since blood is a strong attenuator of light, primarily through optical scattering (Fig. 5(A)), imaging *in vivo* also required development of suitable strategies to overcome this barrier. While the use of an occlusive intravascular balloon to interrupt blood flow is viable in vessels such as the aorta, coronary occlusion carries a significant risk of ischemia and is not acceptable. Instead, first OCT imaging attempts used bolus injections of Ringer's solution (isotonic saline) through the guide catheter. By injecting 8-10 cc through a hand syringe, coronary blood was temporarily displaced and clear OCT imaging of the coronary wall was observed for a few seconds, yielding roughly one dozen cross-sectional frames (Fig. 5(B) and 5(C)). Since the coronaries of swine are disease free, they are highly elastic and significant motion was observed during the cardiac cycle, frequent-

ly giving rise to motion artifacts that manifested as radial offsets between the first axial line of a cross-section and the last radial line (Fig. 5(B) 9 o'clock). This first study found that intra-coronary OCT provided superior resolution compared with IVUS at matching locations and revealed OCT's ability to image the tri-laminar structure of the coronary wall as well as disruptions to this structure that may be associated with stenting, including flaps and dissections. Additionally, high resolution imaging of stents and their apposition to the vessel lumen was demonstrated. Subsequent work integrated the use of an automated injector to better control volume, backing pressure, and flow rate. Following the refinement of the intracoronary imaging procedure, safety was assessed in five swine and an imaging protocol, with selective patient inclusion requirements, was submitted for review by the Massachusetts General Hospital Institutional Review Board. Approval was granted for a pilot study enrollment of 15 human subjects. Intracoronary imaging in human subjects demonstrated unprecedented high-resolution visualization of coronary wall structure, stents and their relation to the wall, and iatrogenic effects of stent deployment such as tissue prolapse [46, 47]. Features of atherosclerotic plaques, as initially identified in the human cadaver studies, were captured in human subjects for the first time [47, 48]. OCT images were spatially co-registered with IVUS images (Fig. 6 and 7) by measuring distances between the imaging plane and landmarks such as side branches and stents in the fluoroscopic recording. Features consistent with the normal, three layered arterial wall (Fig. 6), fibrous plaque (Fig. 6) and thin-capped fibroatheroma and fibrous plaque (Fig. 7) were commonly observed in the first patients. The ability to accurately measure the thickness of fibrous caps overlying lipid-rich plaques is exemplified in Fig. 7, which shows a relatively thick cap (Fig. 7(A), cap thickness 122 ± 7 μm) as well as a very thin cap (Fig. 7(D), cap thickness 20 ± 3μm) [47].
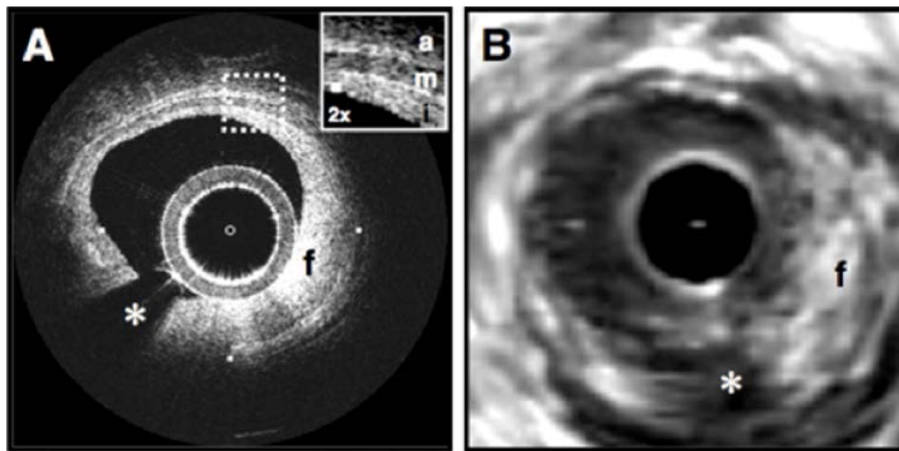

Fig. 6. Fibrous coronary plaque imaged *in vivo* by OCT (A) and IVUS (B). A. From 9 o'clock to 2 o'clock, this OCT image demonstrates visualization of the intima (i, with intimal hyperplasia), media (m), and adventitia (a). The internal and external elastic laminae are visible as signal-rich lines bordering the media (inset). A plaque extending from 2 o'clock to 9 o'clock contains a homogeneous, signal-rich region consistent with a fibrous plaque (f) that is partially obscured by a guide wire shadow artifact (*). B. In the corresponding IVUS image, the fibrous plaque (f) is also visualized. Tick marks, 1 mm. Reprinted from [47].

Following the original human pilot studies, several clinical studies applied intracoronary time-domain OCT to investigate plaque morphology [49–53], stent deployment [48, 54–57], tissue response to stenting [58–62], and thrombus formation and evolution [63].

Despite the encouraging early adoption of time-domain intracoronary OCT as a research tool and the later availability of commercial time-domain systems, there was very little indication of interest in the technology as a routine clinical tool. Even within the research community, there was significant frustration with the duration and difficulty of procedures and the

limited length of coronaries that could be imaged [64]. The primary limitation was in the low image acquisition speed, which was determined by the A-line rate of just a few kilohertz. The recognition that moving to very high speed acquisition would permit even intermittent flushing for comprehensive volumetric coronary artery imaging drove subsequent technical development and revolutionized the field [65].
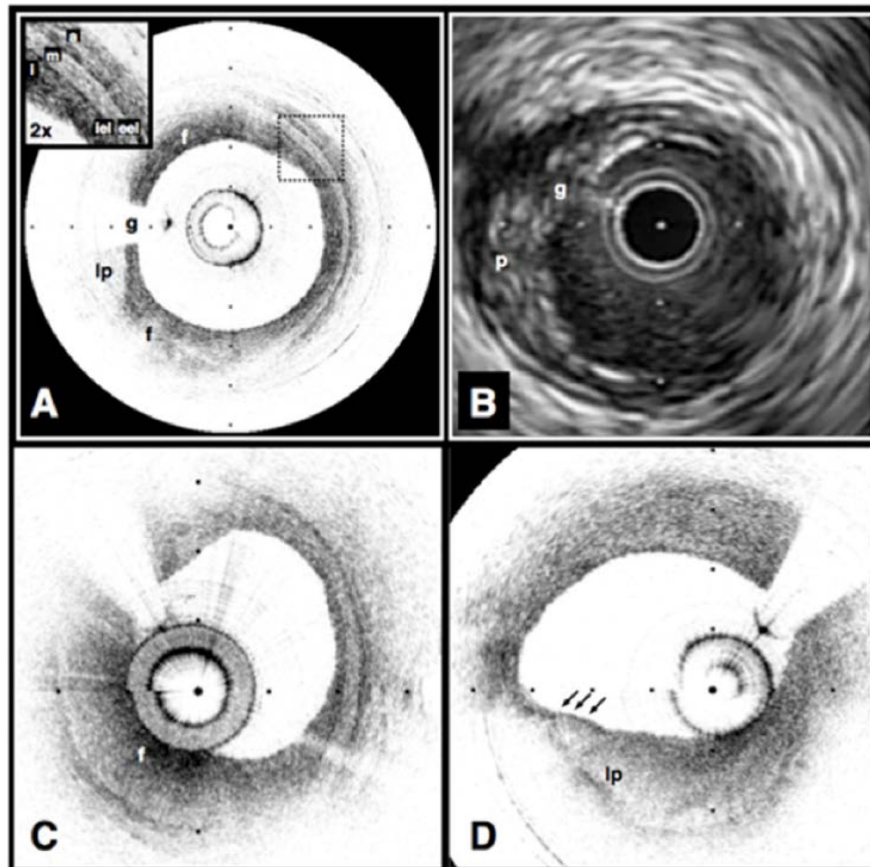

Fig. 7. Echolucent coronary plaque imaged *in vivo* by optical coherence tomography (OCT) (**A**) and intravascular ultrasound (IVUS) **(B). (A)** An atherosclerotic plaque extending from 5 o'clock to 12 o'clock contains regions consistent with fibrous tissue (f) and a homogeneous, signal-poor region (lp), which is partially obscured by a guidewire shadow artifact (g). Fibrous plaque (C), showing characteristic high, homogeneous signal (f). Example of thin-capped lipid-rich plaque (D). Tick marks, 1 mm. OCT displayed in inverse gray scale. Reprinted from [47].

5. Advent of Fourier domain OCT

Although the speed of delay scanning devices continued to improve [66], the sensitivity of OCT was a fundamental barrier to increasing speed significantly. In order to increase the speed 10-fold, signal detection sensitivity would be penalized 10 dB. Despite an early analysis by Gerd Häusler [67], that suggested detection improvements offered by spectral analysis, and despite the demonstration of a spectrometer-based system for ophthalmic imaging [68], there had been no convincing theoretical analysis or experimental demonstration of high-sensitivity, high-speed interferometric imaging prior to 2003. That year, however, three groups independently provided the firm theoretical basis and experimental demonstration of Fourier domain OCT and its enormous sensitivity advantage enabling high-speed imaging [69–72]. This work rapidly led to two alternative embodiments for Fourier domain technolo-

gy: spectrometer based "spectral domain OCT" and wavelength swept laser based "frequency domain OCT". (We note that there isn't complete consensus regarding terminology for the different configurations.) Since silicon camera technology was already mature, spectral domain systems were primarily implemented for near infrared wavelengths, ~800 nm, and applied to ophthalmic imaging. In comparison, InGaAs cameras were less advanced and the lack of high pixel count, fast readout cameras for 1.3 μm operation focused infrared system designs toward the frequency domain approach. For intravascular imaging, the rapid motion of the heart during the cardiac cycle additionally made frequency domain imaging the dominant technology since spectral domain required temporal integration in the spectrometer and is therefore prone to fringe washout [73]. The rapid development of high speed wavelength swept lasers [74–78] drove advances in frequency domain OCT performance, and led to catheter-based systems capable of over 100 frames per second acquisition [65].

5.1 Catheters

Although the imaging performance of catheters based on gradient index lenses was sufficient for cardiovascular applications, the manufacture of the optical cores for these catheters was problematic in terms of assembly time and poor reproducibility from unit to unit. In 2004, an alternative was developed that addressed these challenges and additionally permitted compensation for the astigmatism arising from propagation of light from the optical core through the narrow diameter, cylindrical catheter sheath [79, 80]. The new design took advantage of an optical fiber fusion splicer to create a monolithic element that permitted beam expansion, focusing, and transverse beam redirection. Specifically, a single-mode fiber was spliced to a pure silica, non-guiding fiber, which was then cleaved to a predetermined length. By reinserting the cleaved end into the heating element of the splicer and controlling the heating temperature, duration, and motion of the fiber during heating, a prolate spheroid shape could be produced at the fiber tip (Fig. 8). Subsequent polishing of the tip was used to create an angled facet for total internal reflection. By computer control of parameters, high reproducibility of the focusing specifications could be achieved and it was straightforward to automate the process to create batches of more than 20 optical cores in one setting.
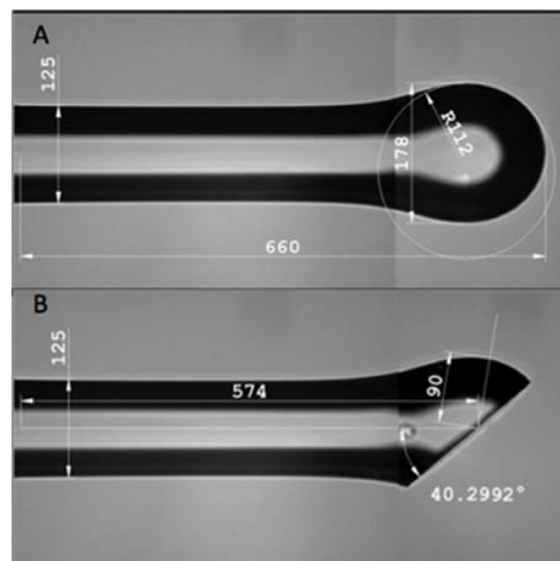

Fig. 8. Prolate spheroid (A) formed at end of silica fiber after splicing to single mode fiber. After polishing (B), total internal reflection directs light emitted from the SMF core to a transverse focal spot. Controlling the radii of curvature of the spheroid permits compensation for the astigmatism arising from the catheter sheath inside which this fiber will be inserted.

5.2 Rotary junction

In order to further simplify the connection of catheters in the sterile field of the cardiac catheterization laboratory and to enable high speed imaging, the optical rotary junction was redesigned (Fig. 9). Using more precise bearings and appropriate motor gearing, this new design permitted catheter rotation at speeds of up to 7,200 RPM and imaging at over 100 images per second [65].
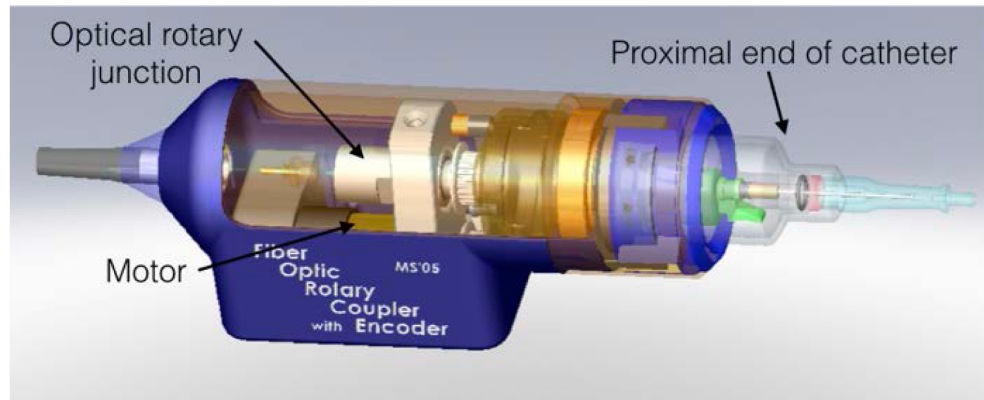

Fig. 9. Rotary junction circa 2005. Connection between the optical rotary junction and the motor was facilitated by a cogged belt. The entire unit was mounted in a conventional IVUS pullback tray for longitudinal scanning.

5.3 Data acquisition

One challenge that was faced in implementing a clinically viable, high-speed frequency domain system was in handling the high data rates that were required for signal recording and processing. Operating at a 60 kHz axial line rate required capturing and storing nearly 1 GB of data per second [65, 81]. This was accomplished by streaming the data from a 2-channel, 200 MS/s digitizer to an array of hard drives. The data was also down-sampled for real time processing of approximately 20 images per second to monitor the imaging procedure.

5.4 Clinical translation

With the completion of the prototype optical frequency domain imaging (OFDI) system, including the redesigned catheter and rotary junction, testing was performed in living swine [65]. In this work, the imaging system operated at 108 frames per second with a pullback speed of 5 mm/s, permitting imaging lengths of up to 6 cm within main coronary arteries under single bolus injections of Ringer's solution. The system included polarization-diverse detection to avoid polarization fading and also used an acousto-optical frequency shifter to remove depth degeneracy [82], and provide an imaging range of 7.3 mm (14.6 mm diameter cross-sections). Normal swine coronary arteries were imaged and images were also acquired following stent deployment allowing visualization of the stent-vessel wall apposition and intimal/medial dissections (Fig. 10). Following acquisition of the OFDI intensity data, segmentations were performed based on the image interpretation criteria defined in Section 3. The individual segmentations were then used to reconstruct a volumetric perspective with red color signifying intima and media, gray denoting adventitia, and blue corresponding to stent struts (Fig. 10).
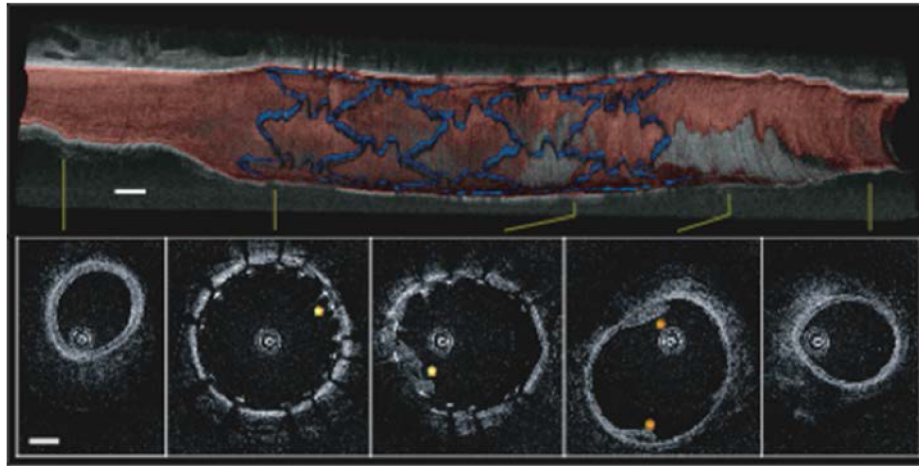
Fig. 10. Volumetric imaging of a stented porcine coronary artery *in vivo* with individual cross-sections from denoted locations. Blue, stent; red, intima and media; gray, adventitia and surrounding tissue. Scale bars, 1 mm. Reprinted from [65].

6. First-in-man studies with Fourier domain intravascular OCT

Following the demonstration of safe intracoronary imaging with high speed frequency domain OCT, an Investigator-sponsored Investigational Device Exemption application was filed with the Food and Drug Administration requesting permission to conduct a first human trial for coronary artery imaging. Upon approval and with subsequent Internal Review Board approval, first human imaging studies were conducted at the Lahey Clinic in Burlington, Massachusetts [83]. Figure 11(B) and 11(D) present images acquired in the first cases, here showing both lipid rich plaque ('L' in Fig. 11(B)) and a calcific nodule ('Ca' in Fig. 11(D)) within a region that had previously been stented. By applying the image interpretation criteria discussed in Section 3, the three-dimensional OCT data sets were segmented according to normal vessel wall, fibrous plaque, lipid-rich plaque, calcific plaque, and stent struts in order to display three dimensional perspectives (Fig. 11(A) and 11(C)) [84].

The initial imaging protocol permitted second time-point imaging in patient who were readmitted to the cardiac catheterization lab for additional, medically-indicated procedures. Figure 12 depicts volumetric images from the right coronary artery of a patient, including two stented regions, on a first time-point scan. Imaging was performed at a pullback speed of 20 mm/s (frame size 1536 radial points x 512 A-lines) and a longitudinal pitch of 200 μm. During the imaging procedure, Ringer's solution was infused at a rate of 3 mL/s through the guide catheter and a 7 cm long data set was recorded in under 4 seconds. Rendering of the data was performed off-line to segment portions of arterial wall, stent, calcium, lipid, and macrophages using the image interpretation criteria of Ref [31]. This case was particularly interesting because the stent (s1 in Fig. 12) had been placed 9 years previously in a stenotic region primarily comprising fibrous plaque and little lipid. This portion of the artery showed no sign of in-stent restenosis, representing a perfect outcome. The region of the second stent (s2), however, comprised a circumferential lipid rich plaque at the border of the stent. Fifteen months after stent s2 was deployed and the images of Fig. 12 were acquired, the patient was readmitted to the hospital with symptoms of unstable angina. Diagnostic angiography indicated stenosis in the right coronary artery approximately at the location of the proximal border of stent s2. Subsequent frequency domain imaging indicated significant plaque growth and deeply embedded stent struts (Fig. 13). This case was thought to be consistent with prior autopsy studies, which had indicated that the most common finding associated with the failure of drug eluting coronary stents was a poor positioning of the stent with respect to a lipid-rich atheroma. Specifically, these studies found that when a drug eluting stent is placed with its edge

within the longitudinal borders of plaque, late restenosis can arise. This scenario points out one potentially vital clinical role for OCT, since it is uniquely well suited to plaque type identification and determining plaque border locations and since angiography alone is clearly incapable of this assessment [85].
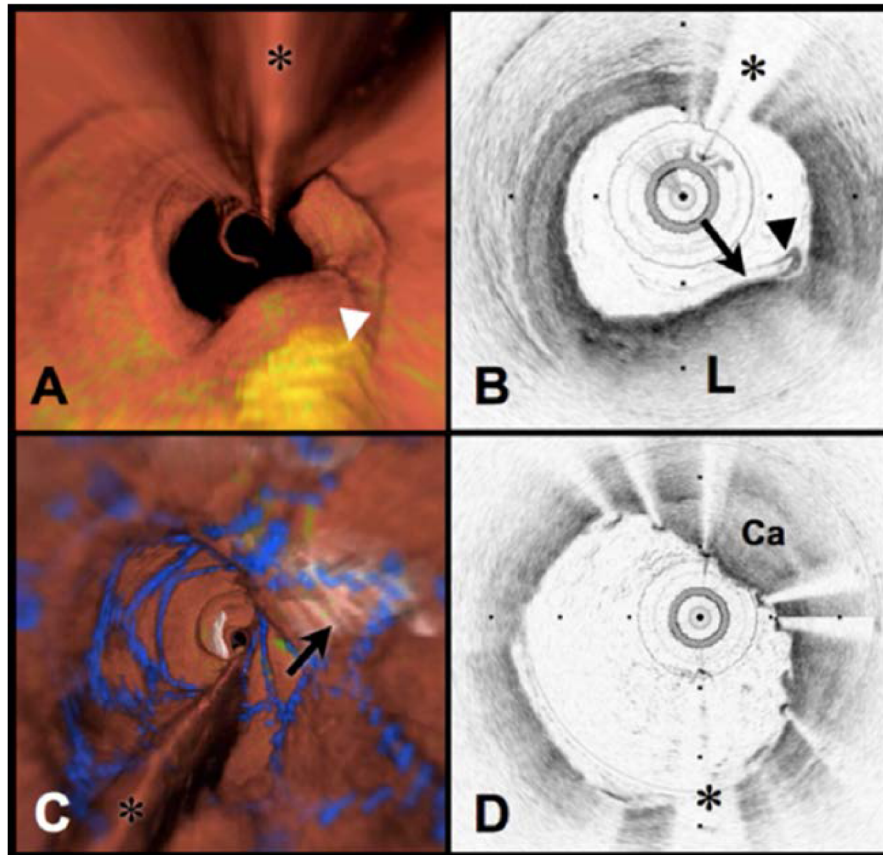

Fig. 11. Volumetric OFDI imaging of the human LAD coronary artery, obtained in vivo. A. Fly-through rendering view (proximal-distal) of the OFDI data set, acquired during a single purge of Lactated Ringers solution (3 ml/s), an imaging catheter pullback rate of 2.0 cm/s and at an image acquisition rate of 100 frames per second. The fly-through depicts a yellow, elevated lipid-rich lesion with scattered macrophages (green). B. OFDI cross-sectional image obtained at the location of the white arrowhead in (A) demonstrates OFDI evidence of a thin-capped fibroatheroma; a lipid pool (L), a thin cap (black arrow), and a dense band of macrophages at the cap-lipid pool interface. A thin flap of tissue (black arrowhead) can be seen over the cap. C. Fly-through view (proximal to distal) shows a calcified lesion (black arrow) beneath a newly deployed stent. D. OFDI cross-sectional image obtained at the location of the black arrow in (C) demonstrates a large calcific nodule (Ca) from 11 to 5 o'clock causing significant stent distortion, highlighted by the shorter inter-strut distances of the overlying stent compared to the opposing vessel wall. Color scale for A and C: red – artery wall; green – macrophages; yellow - lipid pool; blue – stent. Tick marks, 1 mm. OCT displayed in inverse gray scale. * denotes guide wire artifact. Reprinted from [84] with permission from Elsevier.
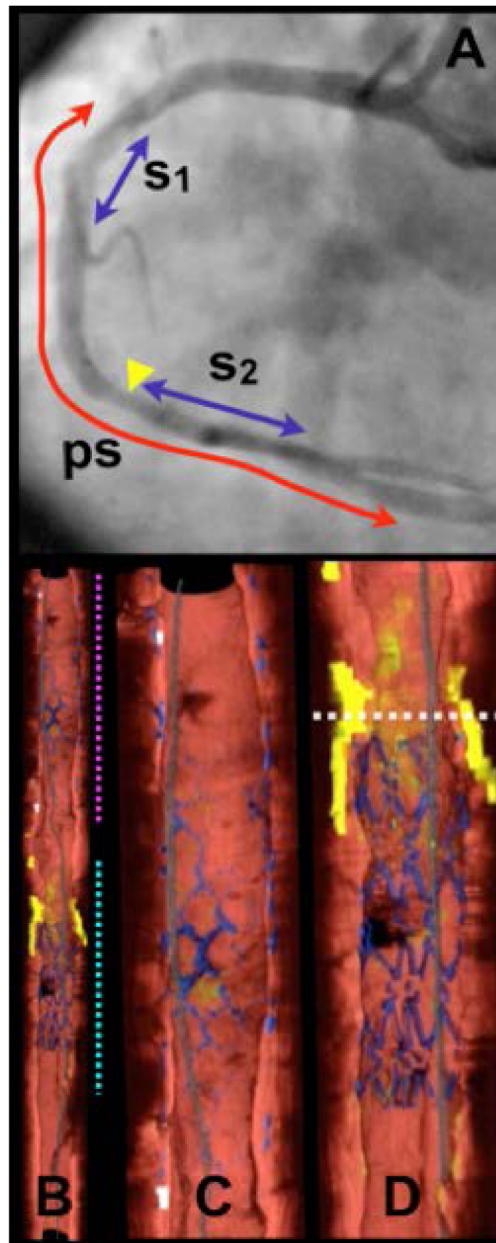
Fig. 12. Images of human right coronary artery acquired *in vivo*. A. Angiogram following stent deployment, showing stent deployed 9 years previously (s1) and stent (s2) that was deployed immediately prior to imaging. 7.0 cm pullback segment (ps). B. Cutaway view of entire three-dimensional volume rendered data set (top – proximal; bottom – distal). C. Expanded view of segment denoted by magenta dotted line in (B), showing stent s1. D. Expanded view of segment denoted by cyan dotted line in (B), showing stent s2. White dotted line in (D) is through a lipid-rich lesion, proximal to s2. Color scale for B - D: red – artery wall; green – macrophages; yellow - lipid pool; blue – stent; gray – guide wire. Reprinted from [83].
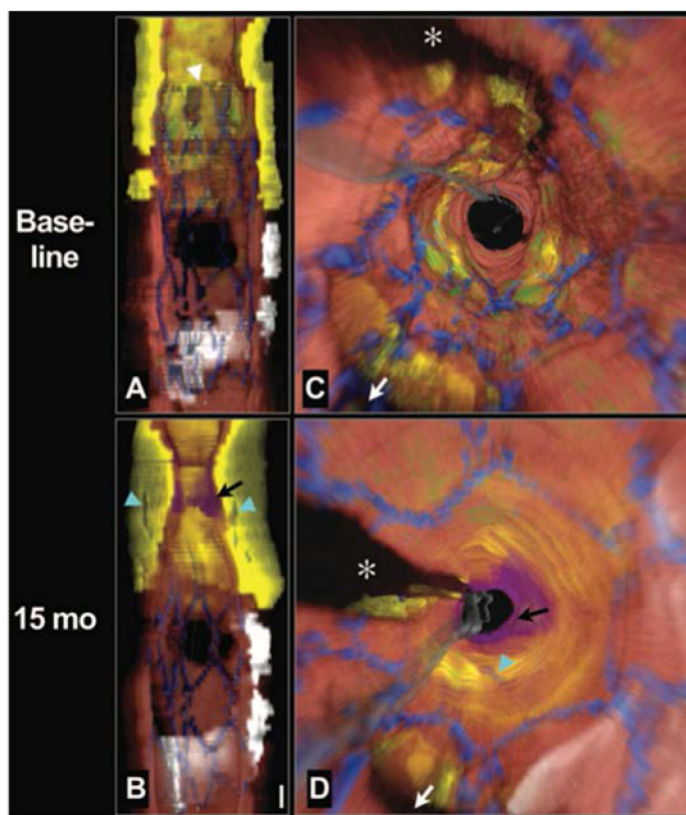
Fig. 13. Longitudinal cutaway view (A) and fly-through view (C) at baseline demonstrates that the stent was deployed over a large circumferential lipid core and that the proximal stent margin was placed in the center of the lesion (white arrowhead). Longitudinal cutaway view (B) and fly-through view (D) at 15 months shows that the necrotic core had grown or prolapsed into the lumen, leaving the struts embedded deep within the plaque (cyan arrows). A thrombus formed near the stent edge (black arrows). Red color indicates artery wall; green, macrophages; yellow, lipid core; blue, stent; white, calcium; purple, thrombus; gray, guide wire. White arrow denotes side branch in (C) and (D). *Guide wire shadow. Scale bar in (B), 1 mm (for both A and B). Fly-through views are presented from a distal to proximal perspective. From *Circulation Cardiovascular Interventions* **3**, 193-196 (2010).

7. Clinical studies

Since the inception of high speed intracoronary frequency domain imaging, the use of this technology as a tool for investigating atherosclerosis and response to drug and device intervention has grown exponentially (Fig. 14). Certainly, the diversity of clinical research with intracoronary OCT would not have been possible without the widespread availability of commercial imaging systems and catheters, which are now provided by St. Jude Medical [86] and Terumo Corporation [87]. The role of plaque type and morphology in acute coronary syndromes (ACS) has been investigated extensively [88–91]. Macrophage density, thought to be associated with collagen degeneration and structural weakening of plaques, was shown to be significantly elevated in patients with ACS [89]. Neovascularization, the growth of vessels within the coronary wall, is an important factor in atherogenesis. OCT studies have shown that neovascularization is associated with thin fibrous caps, muted response to statin therapy, and plaque progression [92–94]. Taking advantage of OCT's high resolution has allowed investigation of fibrous cap morphology in plaque disruption, indicating that cap thinning at the shoulder of atheromas was commonly associated with disruption and that cap disruption tended to be directed against the direction of coronary flow [88, 90, 95]. Another plaque morpho-

logical feature that can be identified by OCT, plaque erosion, is a frequent finding in patients with ACS [96]. Calcific nodules, identified by OCT, were found to be the least common etiology for ACS [96]. Many studies have investigated stent failure and the correlation between failure and features such as stent malapposition and placement of stent borders with respect to lipid rich plaque [97, 98].
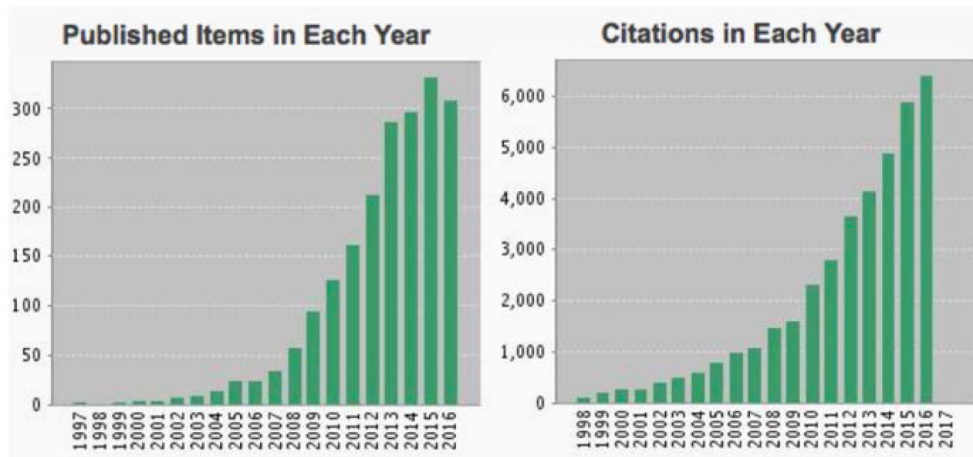

Fig. 14. The number of publications describing research utilizing intravascular OCT for investigating coronary atherosclerosis or response to intervention has grown exponentially since the advent of high-speed imaging with frequency domain technology. From Thomson Reuters, *Science Citation Index Web of Science, November, 2016.*

Recently, many studies have begun to comprehensively test OCT's potential role outside of research as a common tool for the cardiac catheterization lab. Studies have indicated that OCT-guided percutaneous coronary intervention is associated with improved outcome relative to conventional procedures guided by angiography alone [99, 100]. Studies have shown that abnormalities following stenting were frequently found by OCT and that irregular tissue protrusion between stent struts and small minimal stent area were independent predictors of outcome [101, 102]. Although these trials must be confirmed with larger, multicenter studies, they suggest that OCT may, indeed, have a significant future role in routine care for patients undergoing catheterization.

While anticipating future outcomes is speculative due to the many factors that influence the adoption of new technologies, some of the possible roles that OCT may play in cardiology are associated with very high volume usage in the US as well as Europe, Asia, and other countries in North and South America. It is well appreciated that standard angiographic assessment is insufficient to delineate the borders of atheromas and, as a result, stents may be suboptimally with a proximal or distal end within necrotic-core plaque. This "longitudinal geographic miss" can incompletely cover unstable locations resulting in rapid plaque progression and stent failure due to angiographic edge restenosis [85]. Comprehensive plaque characterization and three-dimensional mapping could avoid such complications. Stent selection may also be improved based on plaque classification [103]. If these scenarios come to pass, intravascular OCT could be used in several million cases per year. Current capabilities and specifications of intravascular OCT may be sufficient, but advances that improve resolution and image clarity, increase contrast of tissue composition, or permit imaging to greater depth within thick coronary plaques remain desirable. The following section discusses possibilities on these technological frontiers. We note that advances in image processing could strongly influence clinical adoption through automated interpretation of plaque type or stent features. Seeking to place some reasonable bound on this review, we have not included a description of efforts on this front. Additionally, commercialization of technology is complex; again, due to

page limitations, we have left out a comprehensive discussion of influential factors in this area.

8. Outlook

As described in the foregoing section, intravascular OCT is already established as a primary tool for research, testing new drugs and devices and also for understanding disease. Commercial systems are in widespread use in Japan and are also available in the United States and Europe. There remains an opportunity, however, for innovation to enhance the utility of OCT for cardiovascular imaging. Although the current catheter paradigm of a sheath enclosing a wound wire torque cable is effective, infidelity of rotational speed at the distal transducer is common and results in an image artifact referred to as non-uniform rotational distortion ("NURD"). Recent advances in image and signal processing have found that analyzing the speckle pattern observed in the image can yield an effective means for compensating NURD and improving image quality [104]. Image artifacts associated with cardiac motion during one catheter rotation are modest, but they frequently distort three-dimensional visualizations since their time scale is fast relative to catheter pullback speeds. This problem can be mitigated significantly by further increasing the speed of acquisition, rotation, and pullback and dramatic improvements have recently been experimentally demonstrated [105, 106]. Increased imaging speed is additionally advantageous since it can reduce the volume of flushing agent used to reduce signal attenuation by blood.

As described in Section 3 above, the birefringence of collagen and smooth muscle can be exploited using polarization sensitive OCT. Until recently, however, this capability was restricted to tissue studies *ex vivo* using microscope configurations rather than catheter-based systems. Following the finding that polarization mode dispersion in the OCT interferometer and catheters inhibits accurate and reproducible polarimetry [107], methods were identified to mitigate this effect and enable intravascular birefringence [108, 109] and depolarization [110] measurements. This work has recently been translated into clinical studies with intriguing results demonstrating the very promising utility of polarimetry for vascular and plaque characterization [37, 38]. Figure 15 depicts image data acquired in a human coronary artery *in vivo*. The conventional intensity image (Fig. 15(A)) shows the typical three-layered vessel wall structure from 9 o'clock to 12 o'clock but the contrast of the media relative to the intimal and adventitia is limited. In the birefringence image, however, the high birefringence of the smooth muscle in the media yields pronounced contrast. The heterogeneity of the birefringence within the fibrous plaque (2 o'clock to 5 o'clock) is consistent with heterogeneous collagen distribution as demonstrated in histopathologic correlations obtained *ex vivo*. Within the fibrous plaque, at 3 o'clock, a linear, high signal feature with radial shadow can be seen in the intensity image. In the birefringence image, this location is identified as having high local birefringence and is also seen to give rise to depolarization (DoP cross-section). These features are consistent with the presence of cholesterol crystals, a very interesting finding considering the purported role of such crystals in plaque disruption [39].
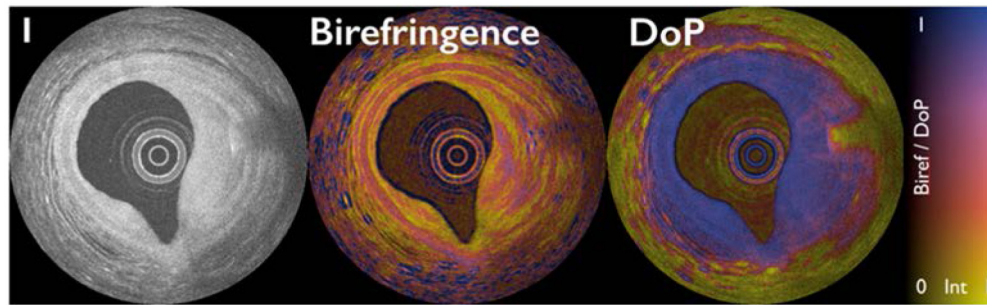
Fig. 15. Intensity image (left), birefringence image (center), and depolarization image (right) of a human coronary artery with plaque. The lookup table encodes polarimetric measurement by color and the intensity data by brightness.

Recent studies have suggested that the combination of deep tissue imaging at low resolution by intravascular ultrasound with the high resolution near lumen imaging of OCT can improve the identification of thin capped fibroatheromas in humans [111]. Although this study was conducted using separate IVUS and OCT catheters, work is progressing toward a single catheter integrating both ultrasound and OCT [112]. Additionally, it is known that the assessment of the physiological significance of stenotic coronary lesions, through estimations of flow impairment, can be an important method for determining optimum intervention. Recent work has suggested that direct flow measurements can be made directly from the OCT data, potentially enhancing the diagnostic information gained by intravascular imaging [113–115]. Other studies have suggested a potential role of OCT for monitoring atrial ablation [116–118].
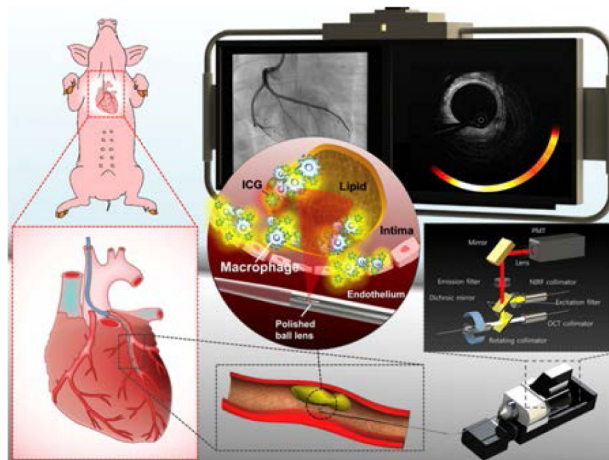

Fig. 16. Optical coherence tomography-near-infrared fluorescence (OCT-NIRF) imaging of high-risk coronary plaque. Intracoronary high- speed OCT-NIRF imaging, a catheter-based fully integrated dual-modal imaging, enables an accurate estimation of high-risk plaques. Along with detailed coronary microstructure by OCT, NIRF imaging provides biological readouts of inflammatory high-risk plaque by assaying indocyanine green-enhanced NIRF from macrophages and lipids. With automated rapid correction of distance-dependent NIRF signals, the imaging system enables real-time, quantitative display of synchronized OCT-NIRF images. Co-registered structural – molecular information could offer more comprehensive assessment of high-risk coronary atheroma and stent biology as well. Reprinted from [121], by permission of Oxford University Press.

Complementing the microstructural information provided by OCT with compositional information such as collagen and smooth muscle identified by polarimetry, can be enhanced

further through the addition of molecular information from exogenous agents and fluorescence. The use of magnetic ironoxide nanoparticles and their magnetomotive response has helped to identify fatty streaks in plaques *ex vivo* [119]. Combining detection of fluorescence with OCT in a multimodal intravascular catheter (Fig. 16) has also been demonstrated, complementing the structural OCT signal with true molecular information [120–123]. These catheters employ a dual clad fiber to collect fluorescence through the inner cladding while operating OCT through the single mode core of the fiber. After initial demonstration in rabbit aorta [120], the autofluorescence of fibroatheromas has been investigated in human patients [122], and the use of indocyanine green (ICG) as a contrast agent to label regions of inflammation and compromised endothelial function has been explored in carotid samples obtained from patients that received an intravenous injection of ICG before endarterectomy [123], and in a swine model of atherosclerosis [121] (Figs. 16 and 17). A discussion of other hybrid modalities is somewhat outside the scope of this review, but interested readers my enjoy another survey that has recently summarized efforts on this front [124].
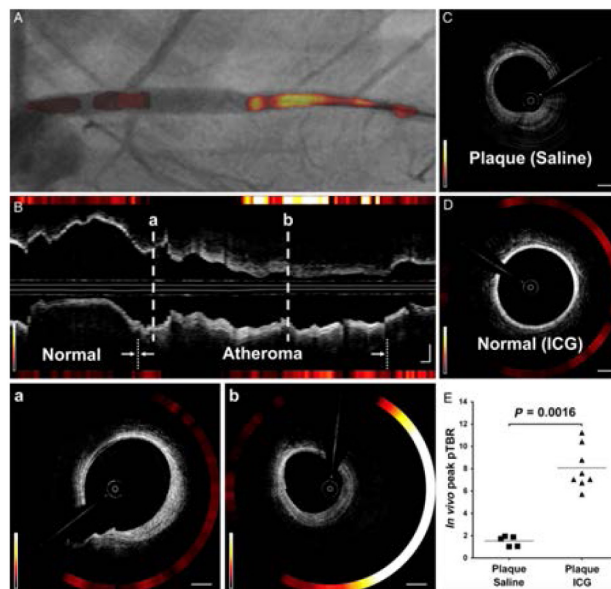

Fig. 17. *In vivo* optical coherence tomography-near-infrared fluorescence (OCT-NIRF) imaging. (A) Image of contoured 2-D NIRF map overlaid on angiography. (B) Corresponding longitudinal OCT-NIRF image. (B a) Weak NIRF activity on fibrotic OCT signal pattern. (B, b) Strong NIRF activity on fibrofatty OCT signal pattern. (C) Saline-injected control. (D) Normal-looking artery. (E) Comparisons of peak pTBR. Equally windowed. Reprinted from [121], by permission of Oxford University Press.

Considering the unique capabilities of OCT, the progress that has been made to date with developing, validating, commercializing, and disseminating intravascular systems, and the advances with its utilization as a powerful research tool for investigating coronary atherosclerosis and the response of disease to intervention, as well as its potential role in routinely guiding interventions, it is clear that this technology will continue to make significant impact in cardiology.

Funding